Multi-omics Reveals Immune Response and Metabolic Profiles during High-Altitude Mountaineering

Jianhua Yin[1,2,9], Jingzhi Lv[1,3,9], Shichen Yang[3,4,9], Yang Wang[3,4,9], Zhuoli Huang[1,3], Xue Wang[4], Guixue Hou[5], Wenwen Zhou[1] , Ying Liu[1,3,4], Weikai Wang[1,3], Xiumei Lin[3,4], Yunting Huang[6], Yuhui Zheng[1,3], Chen Wei[1,3], Yue Yuan[1,4], Yaling Huang[1,4], Chang Liu[1,4], Haoran Tao[5], Huanhuan Liu[1], Ruquan Liu[1], Yan Zhang[1], Guodan Zeng[1], Peng Gao[2,5], Longqi Liu[1,2,3,4], Jun Cao[5,*], Chuanyu Liu[1,2,4,*], Xin Jin[1,2,7,*], Jian Wang[1,8*]

[1]BGI Research, Shenzhen 518103, China

[2]Shanxi Medical University - BGI Collaborative Center for Future Medicine, Shanxi Medical University, Taiyuan 030001, China

[3]College of Life Sciences, University of Chinese Academy of Sciences, Beijing 100049, China

[4]BGI Research, Hangzhou 310030, China

[5]BGI, Shenzhen 518083, China

[6]China National GeneBank, BGI Research, Shenzhen 518120, China

[7]School of Medicine, South China University of Technology, Guangzhou 510006, China

[8]James D. Watson Institute of Genome Sciences, Hangzhou 310058, China

[9]These authors contributed equally

*Correspondence: caojun@genomics.cn (J.C.); liuchuanyu@genomics.cn (C.L.); jinxin@genomics.cn (X.J.); wangjian@genomics.cn (J.W.)

SUMMARY

The physiological perturbations induced by high-altitude exposure in mountain climbers, manifesting as metabolic and immunologic deviations, have been previously reported but are not fully understood. In this study, we obtained longitudinal multi-omic profiles of blood samples for healthy mountain climbers during two mountaineering stages (acclimatization and extreme altitude mountaineering). Our integrative assay included metabolomics and lipidomics profiling of plasma coupled with single-cell transcriptomic analysis of 375,722 immune cells. Longitudinal analysis revealed dynamic immune response profiles, during the acclimatization period, characterized by the downregulation of inflammatory responses in monocytes and classical dendritic cells (cDCs) and an increase in the proportion of cytotoxic $CD8^+$ T cells with enhanced immune effector processes. In contrast, during extreme altitude mountaineering, the activation of inflammatory responses and impairment of T cell effector function were observed, concomitant with an increased cellular response to hypoxia and oxidative stress pathways. Furthermore, we found upregulated glycolysis and antioxidant gene expression during extreme altitude mountaineering, which was primarily orchestrated by *HIF1A* and *NFE2L2*, while decreased expression of these genes was observed in dysregulated plasmacytoid dendritic cells (pDCs). Finally, high-resolution plasma metabolic analysis revealed significant alterations in the metabolism of climbers, involving enhanced glutamine and fatty acid metabolism.

INTRODUCTION

High-altitude mountaineering, with the main objective of reaching a summit, is a challenging and potentially dangerous activity. Increased accessibility to high mountains has led to the growing popularity of mountaineering[1]. Mountain climbers are confronted with harsh environmental conditions upon exposure to high altitudes, among which the most crucial variable is hypoxia owing to the progressive decline in barometric pressure with increasing altitude[2]. Several physiological responses are initiated in climbers to adapt to reduced oxygen availability, such as enhanced ventilatory response, increased cardiac output, and improved tissue oxygen extraction[3]. The combination of hypoxia and intense physical activity may impose greater physiological and metabolic demands on mountain climbers[4]. Notably, mountain climbers are susceptible to a range of health issues, including altitude illness[3], body mass loss[5], immune dysfunction and increased vulnerability to infections[6]. Among them, immunological and metabolic outcomes are key mediators, but the underlying mechanisms remain incompletely characterized.

Moderate exercise is beneficial for immune function, while an excessive duration and intensity of exercise may lead to immunological impairment[7, 8]; therefore, it is crucial to understand the immune outcomes of different types of exercise. Previous studies have reported that low oxygen availability at high altitudes has a significant impact on the abundance and function of immune cells; specifically, it leads to the downregulated expression of innate immune-related genes[9], a reduction in the proportion of plasmacytoid dendritic cells (pDCs)[10], and a decrease in $CD3^+$ T lymphocytes[11]. Importantly, exercise at high altitudes may intensify the extent of hypoxia, further impeding immune function[4] and elevating the levels of inflammation and oxidative stress[12-14]. Notably, exercise has the potential to reprogram immune cell metabolism through alterations in oxygen availability, the regulation of cellular energy sensors, and the accumulation of immunometabolic regulators[4, 15]. Previous studies have assessed the metabolic activity of immune cells during high-altitude exercise by assessing metabolism-related parameters, including reactive oxygen species (ROS), mitochondrial activity, and intracellular calcium ions[16, 17]. These metabolic changes may subsequently impact the immune cell state and cell fate[18]. However, the underlying mechanism of the immune response to high-altitude mountaineering remains elusive. In addition, in a previous study, participants who ascended to high altitudes

91 exhibited substantial alterations in plasma metabolic molecules[19]. A comprehensive
92 characterization of both immune cells and plasma analytes from mountain climbers is needed to
93 fully understand the dynamic alterations in the immune response and plasma metabolites.
94
95 The emergence of single-cell RNA sequencing (scRNA-seq) has facilitated an in-depth
96 dissection of immune response changes driven by exercise and has been applied to exercise
97 immunology[20]. To elucidate the immune response and metabolic alterations during high-altitude
98 mountaineering, we performed multi-omics profiling, including targeted metabolomics and
99 lipidomics of plasma, as well as single-cell transcriptome analysis of circulating immune cells, on
100 each sample from eleven mountain climbers (Figure 1A). In this study, our longitudinal analysis
101 revealed dynamic immune responses at different stages of high-altitude mountaineering. In
102 particular, we identified a crucial immune adaptive response mediated by the transcription factors
103 (TFs) *HIF1A* and *NFE2L2* during extreme altitude mountaineering. Furthermore, substantial
104 alterations in plasma metabolites, including increased glutamine metabolism and fatty acid
105 metabolism, were also observed during high-altitude mountaineering. Overall, the results from this
106 study improve our understanding of the dynamic immune and metabolic landscapes elicited by
107 high-altitude mountaineering.
108
109 **RESULTS**
110 **Effects of high altitude on physiological parameters in mountain climbers**
111 This study was conducted during an expedition to the Muztagh Ata peak (7546 m) with the aim of
112 investigating the dynamic physiological, metabolic, and immune responses of mountain climbers
113 at high altitudes. Eleven climbers (8 males, 3 females) with a mean age of 37.4 ± 11.4 years and a
114 mean body mass index (BMI) of 23.60 ± 3.16 kg/m^2 were recruited (Table S1). After reaching
115 1289 m on D1, the mountaineering experimental plan consisted of two stages: the period of
116 acclimatization (D2-D8) and then the period of extreme altitude mountaineering (D9-D16) (Table
117 S1). A total of 10 physiological phenotypic indexes, including blood oxygen saturation (SpO_2),
118 heart rate (HR), Lake Louise score (LLS), body composition, and routine blood and ultrasensitive
119 C-reactive protein (CRP) tests, were assessed for eleven climbers (Figure 1A). Furthermore, 55
120 peripheral blood samples were collected longitudinally at five different time points of

121 mountaineering: D1 (altitude, 1289 m; SpO_2, 95%), performed in low altitudes as a baseline
122 control; D4 (altitude, 4400 m; SpO_2, 82%) and D9 (altitude, 5500 m; SpO_2, 72%), performed
123 following acclimatization to high altitudes of 4400 m and 5500 m; and D11 (altitude, 3200 m) and
124 D16 (altitude, 1289 m), performed after reaching extreme altitudes of 6300 m and 7546 m (Table
125 S1).
126
127 We first analyzed the variations in SpO_2 and HR during different stages of high-altitude
128 mountaineering. Overall, we observed a progressive decrease in the SpO_2 of climbers with
129 increasing altitude and a compensatory increase in the HR from 72 to 105 min^{-1}, with high
130 consistency among climbers (Figure 1B and S1A). When the mountain climbers were exposed to
131 extreme altitudes of 6,300 m and 6,900 m, the SpO_2 decreased to 72% and 69%, respectively.
132 However, in comparison to the initial exposure at 4400 m on D3, we observed a significant
133 increase in SpO_2 from 86% to 93% on D11 following acclimatization, accompanied by a notable
134 decrease in HR from 94 min^{-1} to 71 min^{-1}; such trends were also observed upon re-exposure to an
135 altitude of 5,500 m (Figure S1B). These data indicated that the mountain climbers may have
136 acclimatized to the reduced oxygen levels at very high altitudes (3,500-5,500 m) following the
137 acclimatization period (D2-D8). Next, we compared the changes in body composition
138 characteristics, including BMI, body fat percentage (BFP%), muscle mass (MM, kg) and fat mass
139 (FM, kg), and no significant changes were observed in these parameters (Figure S1C). In addition,
140 routine blood tests and CRP analysis were performed before (D1) and after (D16) the
141 mountaineering expedition (Figure 1A). The results showed a significant increase in the numbers
142 of neutrophils (NEUT) and monocytes (MONO) on D16 compared with those at baseline (D1)
143 (Figure 1C). Moreover, we detected a significant increase in the level of CRP (Figure 1C), a
144 marker of the inflammatory response, consistent with previous reports that long and arduous
145 trekking at high altitudes leads to an increase in the inflammatory response[5]. Notably, the
146 proportion of lymphocytes significantly decreased on D16 (Figure S2). In general, the
147 mountaineering expedition induced dynamic changes in multiple physiological phenotypes, which
148 initially confirmed the hypoxic state of mountain climbers at high altitudes and further reflected
149 the impact of high-altitude mountaineering on immune responses.
150

151 **Multi-omics profiling of plasma and peripheral immune cells in mountain climbers**

152 Whole blood samples were collected from eleven healthy volunteers at five different time points
153 during mountaineering. Subsequently, the blood samples were separated: the upper plasma was
154 subjected to metabolomic and lipidomic analyses, and the isolated immune cells were subjected to
155 scRNA-seq analysis (Figure 1A). We analyzed the plasma metabolome and lipidome to obtain a
156 global view of the body's metabolic status, and targeted analysis was performed via ultra-
157 performance liquid chromatography-tandem mass spectrometry (UPLC-MS/MS). After data
158 preprocessing, a total of 309 metabolites and 717 complex lipids were measured per sample, and
159 the list containing all the metabolic analytes can be found in Table S2 and S3. Then, our focus
160 shifted toward metabolites and lipids that were significantly affected by high-altitude
161 mountaineering. The variable importance in projection (VIP) score was used to estimate the
162 differentially abundant metabolites and lipids with the greatest variation in the data; ultimately,
163 348 significantly changed analytes were selected. Extensive perturbations of these molecules were
164 observed at different time points (Figure 1D). Overall, the preliminary findings indicated that the
165 metabolism of climbers underwent substantial alterations.

166

167 We next performed a single-cell transcriptomics analysis of circulating immune cells obtained
168 from mountain climbers to comprehensively characterize the alterations in the immune response
169 induced by mountaineering. After quality control, a total of 375,722 single cells were obtained
170 with an average of 1,083 genes per cell (Figure S3A). The number of cells in each sample ranged
171 from 48,686 to 100,271, and the number of cells at each time point ranged from 12,853 to 55,231
172 (Figure S3B). Then, uniform manifold approximation and projection (UMAP) for dimensionality
173 reduction was employed, and we manually annotated cells based on the expression of classical
174 markers (Figure S4A). In total, 15 major cell types were identified, namely, naive $CD4^+$ T cells,
175 memory $CD4^+$ T cells, naive $CD8^+$ T cells, cytotoxic $CD8^+$ T cells, mucosal-associated invariant
176 T (MAIT) cells, natural killer (NK) cells, proliferating T cells, naive B cells, memory B cells,
177 plasma B cells, $CD14^+$ monocytes, $CD16^+$ monocytes, classical dendritic cells (cDCs), pDCs and
178 platelets (Figure 1E). Next, we calculated changes in the relative proportions of these major cell
179 subpopulations among the circulating immune cells at each time point. The proportion of naive
180 $CD4^+$ T cells decreased significantly on D4, accompanied by a sustained increase in the proportion

181 of memory $CD4^+$ T cells on D11 and D16 (Figure 1F). In contrast, the abundance of NK cells
182 initially exhibited a significant increase on D4, followed by a gradual decrease (Figure 1F).
183 Several subpopulations also exhibited notable reductions at later time points, including the
184 proportion of $CD14^+$ monocytes on D11 and the proportions of cytotoxic $CD8^+$ T cells and pDCs
185 on D16 (Figure 1F, S4B-S4D). These results indicated that the composition of circulating immune
186 cells in mountain climbers significantly changed during high-altitude mountaineering.
187
188 **Altered inflammatory response in monocytes and DCs**
189 Previous studies have demonstrated that high-altitude mountaineering induces an increase in the
190 inflammatory response[12]. Considering the critical roles played by myeloid cells in inflammation,
191 we initially investigated their transcriptional alterations during mountaineering. All monocytes
192 and DCs were subclustered (n=33,577) and classified into nine subpopulations based on the
193 expression of classical marker genes, including three $CD14^+$ monocyte ($CD14^+$ Mono) subgroups:
194 $FCN1^+$ $CD14^+$ Monos, $CCL3^+$ $CD14^+$ Monos and IFN^+ $CD14^+$ Monos; three $CD16^+$ monocyte
195 ($CD16^+$ Mono) subgroups: IFN^+ $CD16^+$ Monos, $CD16^+$ Monos and $C1^+$ $CD16^+$ Monos; and three
196 DC subgroups: cDC1s, cDC2s and pDCs (Figure 2A and 2B). Remarkable alterations in the
197 relative proportions of these subgroups were observed: $CCL3^+$ $CD14^+$ Monos significantly
198 decreased on D4 and D9, followed by a subsequent recovery and significant expansion on D16,
199 and $FCN1^+$ $CD14^+$ Monos significantly decreased on D11 and D16 (Figure 2C). The proportion of
200 $CD16^+$ Monos significantly increased on D4 and D9, followed by a decreasing trend. Furthermore,
201 the proportion of cDC2s significantly increased on D11, while the proportion of pDCs
202 significantly decreased on D16 (Figure 2C, S5A and S5B).
203
204 To gain insight into the functional changes in different monocyte and DC subgroups during
205 mountaineering, we performed differentially expressed genes (DEGs) analysis (D1 was used as
206 the control group) (Table S4). Gene Ontology (GO) enrichment analysis of these DEGs revealed
207 significant enrichment in pathways related to innate immunity, cytokine production, cellular
208 chemotaxis, hypoxia and the inflammatory response in $CCL3^+$ $CD14^+$ Monos, $FCN1^+$ $CD14^+$
209 Monos, $CD16^+$ Monos and cDC2s (Figure S5C). We also performed pathway score analysis to
210 investigate the dynamic changes in key pathways in each myeloid cell subgroup during

211 mountaineering. The expression of genes involved in the innate immune response, inflammatory
212 response, NF-κB signaling and hypoxia pathway was downregulated on D4 and D9, followed by
213 significant upregulation on D11 and D16 in most myeloid cell subgroups, except for pDCs (Figure
214 2D). The expression of *S100A8* and *S100A9* in CCL3^{+} CD14^{+} Monos was significantly
215 upregulated on D4 and then downregulated (Figure 2E). *S100A8* and *S100A9* have been identified
216 as important endogenous damage-associated molecular pattern (DAMP) molecules, which are
217 early amplifiers of the innate immune response to danger signals[21]. Additionally, the expression
218 of multiple genes involved in inflammation were significantly downregulated on D4 and D9 but
219 upregulated on D11 and D16 in CCL3^{+} CD14^{+} Monos, CD16^{+} Monos, cDC2s and FCN1^{+} CD14^{+}
220 Monos, including cytokine-related genes (*TNF*, *CCL3* and *CCL4*); central transcription factors of
221 inflammatory response NF-κB subunits (*NFκB1* and *REL*); and inflammasome activation-
222 associated genes (*NLRP3* and *IL1B*) (Figure 2E and S5D). The activation of the NLRP3
223 inflammasome is triggered by a variety of upstream signals, including mitochondrial dysfunction,
224 metabolic changes and ROS[22]. These observations suggested that high-altitude mountaineering
225 induced dynamic changes in inflammatory responses.
226
227 Next, we analyzed the dynamic changes in TF regulon activity in monocytes and DCs at
228 different stages using single-cell regulatory network inference and clustering (SCENIC)[23]. The
229 regulon activities of multiple TFs, such as inflammation and stress-related TFs (*FOS*, *JUN*, *JUNB*,
230 *FOSB*, *CEBPD*, *BHLHE40*, *NFκB1*, *NFκB2* and *RELB*), decreased on D4 and D9 but increased on
231 D11 and D16 (Figure 2F). A positive correlation between the hypoxia score and inflammatory
232 response score was observed (Figure 2G), suggesting that hypoxia may be a key factor in
233 regulating and activating inflammatory responses during mountaineering. Notably, the expression
234 levels of genes related to the hypoxia pathway and *HIF1A* were significantly increased on D11
235 and D16 (Figure 2D and 2H). Hypoxia induces the upregulation of *HIF1A* expression, leading to
236 the activation of HIF signaling and increased transcription of *NF-κB,* which serves as a
237 downstream target of HIF[24], consistent with previous studies showing that *HIF1A* is essential
238 for regulating the inflammatory response in myeloid cells[25].
239

240 **Dysregulation of pDCs in mountain climbers**

241 The proportion of pDCs in mountain climbers exhibited a striking reduction on D16 (Figure 2C).
242 pDCs can produce type I interferons (IFNs), secrete cytokines and chemokines, and capture and
243 present antigens, thereby playing an important role in immunity to infections[26]. We investigated
244 the changes in the molecular features of pDCs during high-altitude mountaineering, and DEGs and
245 pathway enrichment analysis revealed that the downregulated DEGs were enriched mainly in the
246 following pathways: 'viral process', 'antigen processing and presentation', 'response to unfolded
247 protein', and 'oxidative phosphorylation' (Figure S6A). The downregulated DEGs during
248 mountaineering mainly included the IFN- α regulatory genes *IRF4* and *IRF7*, antigen
249 presentation-related human leukocyte antigen (HLA) class II genes (*CD74*, *HLA-DRB5*, *HLA-*
250 *DRB1*, *HLA-DRA*, *HLA-DQB1*, *HLA-DRP1* and *HLA-DPA1*), and the chemokine receptors
251 *CXCR3* and *CXCR4* (Figure S6B). *CXCR3* and *CXCR4* play essential roles in the migration of
252 pDCs from peripheral blood to infection sites[26]. In addition, we found that multiple DEGs
253 related to protein secretion, such as S*EC61B*, *LMAN2*, *SSR3*, and *PDIA6*, were markedly
254 downregulated (Figure S6B). Therefore, the observed reduction in the proportion of pDCs
255 accompanied by the decrease in the expression level of key genes suggested that pDCs may
256 experience functional impairment during high-altitude mountaineering.

257

258 Next, we explored the changes in the regulon activity of TFs in pDCs using SCENIC. The
259 regulon activities of multiple TFs, such as inflammation- and stress-related TFs (*JUND*, *FOS* and
260 *KLF6*), the IFN-related TF *IRF7* and the unfolded protein response (UPR)-related TFs *XBP1* and
261 *ATF4*, began to decrease on D9 (Figure S6C). *IRF7* is a major transcriptional regulator of the
262 production of type I IFNs in pDCs. *XBP1* is essential for pDC development and survival, and a
263 lack of *XBP1* markedly reduces the size of the pDC compartment[27]. It was speculated that
264 hypoxia may be a negative regulator of pDCs, which is consistent with previous studies showing
265 that the proportion of pDCs significantly decreased under hypoxic conditions[10, 28]. Marked
266 downregulation of the hypoxia pathway was detected in pDCs during mountaineering (Figure 2D).
267 In particular, compared with other monocytes and cDCs, pDCs showed lower expression of
268 *HIF1A* on D11 and D16 (Figure 2H), and in vitro studies have shown the essential role of *HIF1A*
269 in type I IFN production by DCs[29]. Taken together, our findings indicate that mountain climbers

may experience pDC dysregulation.

Dynamic characterization of T and NK cell subsets during high-altitude mountaineering

T cell- and NK-cell-mediated immunity is one of the core immune functions, and we explored their functional changes during mountaineering. All $CD8^+$ T, $CD4^+$ T and NK cells were subclustered and classified into 20 subpopulations based on the expression of classical marker genes, including nine subgroups of $CD8^+$ T cells and nonclassical T cells (n=135,616): naive $CD8^+$ T cells, $CD8^+$ effector memory T cells ($CD8^+$ Tems), $CD8^+$ central memory T cells ($CD8^+$ Tcms), cytotoxic $CD8^+$ T cells, terminal effector-like $CD8^+$ T cells (TE-like $CD8^+$ T cells), γδT cells, MAIT cells, proliferating T cells and NK-like T cells (Figure 3A and 3B); six $CD4^+$ T cell subgroups (n=79,847): naive $CD4^+$ T cells, IFN^+ $CD4^+$ T cells, $CD4^+$ central memory T cells ($CD4^+$ Tcms), T helper 2 cells (Th2 cells), Th17-like T cells and $CD4^+$ regulatory T cells (Tregs) (Figure S7A and S7B); and five NK cell subgroups (n=69,673): $CD56^+$ NK cells, active $CD16^+$ NK cells, $CD16^+$ NK cells, $ZEB2^+$ NK cells and type 1 innate lymphoid cells (ILC1s) (Figure S7C and S7D). The abundances of the T and NK cell subgroups exhibited significant alterations during different periods of mountaineering (Figure 3C and S8A-S8D). The proportion of Tregs, the major suppressors of immune responses, was significantly increased on D9 (Figure 3C), and Tregs play crucial roles in the functional homeostasis of the immune system[30]. The proportion of naive $CD4^+$ T cells decreased on D11, and that of Th2 cells increased on D11 (Figure 3C and S8D). Pathway analysis revealed that the T cell activation pathway was markedly activated in naive $CD4^+$ T and Th2 cells on D11 and D16 (Figure S7E). These results suggested that Th2 cells may be activated during extreme altitude mountaineering.

Notably, the proportions of cytotoxic $CD8^+$ T, γδT and $CD16^+$ NK cells exhibited similar variation trends: the proportion of cytotoxic $CD8^+$ T cells increased on D4 but maintained a decreasing trend afterward and decreased to a minimum on D16 (Figure 3C). To investigate the dynamic changes in the functionality of these T and NK cells during different mountaineering stages, we identified DEGs (Table S5) and performed pathway analysis (Figure 3D). Overall, the pathway scores related to cytotoxicity, T cell activation, the immune effector process and the T cell receptor signaling pathway increased on D4 but significantly decreased on D11 and D16

300 (Figure 3D). Notably, the expression levels of cytotoxic genes (*GZMA*, *GZMK*, *GZMH* and *NKG7*)
301 were also significantly reduced in cytotoxic CD8$^+$ T, γδT and CD16$^+$ NK cells on D11 and D16
302 (Figure 3E). Furthermore, the expression of *KLRD1,* which mediates inhibitory receptor signaling
303 in T and NK cells, was significantly downregulated on D11 and D16 in cytotoxic CD8$^+$ T, γδT and
304 CD16$^+$ NK cells (Figure 3F). Previous reports demonstrated that the deficiency of CD94 encoded
305 by *KLRD1* resulted in susceptibility to lethal viral disease[31]. The expression of the chemokine
306 receptor *CX3CR1*, which is expressed on cytotoxic T cells and NK cells and is thought to
307 participate in T cell migration and immune memory formation[32], was significantly upregulated
308 on D4 and D9 and downregulated on D11 and D16 in cytotoxic CD8$^+$ T, γδT and CD16$^+$ NK cells
309 (Figure 3F). The expression of *CD160*, an activating receptor expressed by NK cells and a
310 functional regulator of cytokine production by NK cells[33, 34], was significantly downregulated
311 in CD16$^+$ NK cells on D11 and D16 (Figure 3F). We also observed significant upregulation of the
312 expression of the immunoregulatory gene *TGFB1* in cytotoxic CD8$^+$ T cells and γδT cells on D11
313 and D16 (Figure 3F); this gene inhibits the differentiation and activation of T cells[35]. Overall,
314 we observed enhanced phenotypes of cytotoxic CD8$^+$ T, γδT and CD16$^+$ NK cells on D4 during
315 the period of acclimatization. However, on D11 and D16 during extreme altitude mountaineering,
316 these cell populations exhibited altered phenotypes characterized by the downregulated expression
317 of effector process-associated genes and the upregulated expression of the immunosuppressive
318 molecule *TGFB1*.
319
320 Additionally, we identified activated CD8$^+$ Tems that exhibited increased expression levels of
321 activation-associated transcripts such as *CD69*, *CXCR4* and *JUN* (Figure 3B). Notably, the
322 proportion of CD8$^+$ Tems was significantly increased on D11 and D16 (Figure 3C). An elevated
323 proportion of CD8$^+$ CD69$^+$ T cells has been previously reported following high-altitude trekking
324 and is considered a beneficial response to immune perturbation[17]. To further investigate the
325 transcriptional changes in CD8$^+$ Tems during mountaineering, DEG and pathway analyses were
326 performed. The pathway scores associated with T cell activation and cytotoxicity were increased
327 on D4 but were significantly decreased on D11 in CD8$^+$ Tems (Figure 3D). The expression of
328 *CD69*, a classical marker of T cell activation, was significantly increased on D9 and D11 (Figure
329 3F). Along with the potential activation of CD8+ Tems, the expression of the cytotoxic serine

330 protease *GZMB*, the antigen presentation-related HLA II class molecule *HLA-DRB5* and the *NF-*
331 *κB* subunit *REL* was significantly upregulated on D11 and D16 in $CD8^+$ Tems (Figure 3E and 3F).
332
333 Next, we analyzed the changes in TF regulon activity in $CD8^+$ T and NK cells at different stages
334 using SCENIC. The regulon activities of a set of TFs associated with inflammation and stress,
335 including *JUN*, *REL*, *ATF3*, *ATF5* and *BHLHE40*, were obviously decreased on D4 and D9 but
336 enhanced on D11 and D16 (Figure 3G). Notably, the regulon activities of *TBX21* and *EOMES*
337 increased on D4 and then obviously decreased, especially on D16 (Figure 3G and 3H). *TBX21* and
338 *EOMES* are highly expressed in $CD8^+$ T and NK cells[36] and regulate the expression of
339 downstream genes, such as *GZMA*, *CCL5*, *NKG7*, *CD160* and *SPON2* (Figure S7F). The regulon
340 activities of *TBX21* and *EOMES* may be suppressed during extreme altitude mountaineering. In
341 general, these results suggested that mountain climbers may experience impaired functionality in
342 cytotoxic $CD8^+$ T, γδT and $CD16^+$ NK cells on D11 and D16.
343
344 **Enhanced unfolded protein response in plasma B cells during high-altitude mountaineering**
345 B cells play an important role in humoral immunity. We subclustered 54,546 B cells and
346 annotated them into eight subgroups based on the expression of classical marker genes, including
347 six B-cell subsets (naive B cells, IFN^+ B cells, activated B cells, memory B cells, $FCRL3^+$ B cells
348 and $SOX5^+$ B cells) and two plasma cell subsets (plasma B cells and proliferating plasma B cells)
349 (Figure 4A and 4B). Then, we analyzed the compositional changes in different stages and
350 observed a significant reduction in the proportion of naive B cells on D4, accompanied by a
351 significant increase in activated B cells. The plasma B cells and other B cell subgroups did not
352 exhibit statistically significant changes (Figure 4C, S9A and S9B). To reveal the functional
353 changes in B cells in mountain climbers, we performed DEG analysis (Table S6). The expression
354 of HLA class II genes (*HLA-DRB5* and *HLA-DQA2*) in activated B cells significantly increased
355 during mountaineering, indicating an augmentation of B cell-mediated antigen presentation
356 capabilities (Figure 4D). In addition to the marked increase in the expression level of *CD69*, we
357 also discovered a significant upregulation of *CD83* on D11 and D16 (Figure 4D), which is
358 important for B cell activation[37].
359

360 To further investigate the functional changes in plasma B cells during mountaineering, DEG
361 analysis was performed (Table S6). Pathway enrichment analysis revealed that the upregulated
362 DEGs were mainly enriched in pathways related to protein folding and the UPR (Figure 4E). The
363 UPR pathway is an essential component of plasma B cell differentiation, and plasma B cells
364 employ a specialized UPR dependent on the IRE1-XBP1 axis for protein synthesis[38]. The
365 expression of *ERN1* (also known as IRE1), a major sensor of the UPR, was significantly
366 upregulated on D11 and D16 (Figure 4F). The expression of *XBP1* significantly increased on D9
367 and D11 (Figure 4F). Additionally, we observed prominently upregulated expression of protein
368 secretion-related genes (*LMAN1*, *HSPA5*, *SSR3* and *PDIA4*) and the immunoglobulin genes
369 *IGHA1* and *JCHAIN* (Figure 4F). The activation of the UPR in plasma B cells potentially
370 contributes to the enhancement of the antibody secretion response in mountain climbers, which is
371 consistent with the reported increase in immunoglobulin levels at high altitudes[39].
372
373 The development of plasma B cells requires the involvement of specific TFs. We also identified
374 *XBP1* in plasma B cells using SCENIC, and the regulon activity of *XBP1* was upregulated on D9
375 and D11 (Figure 4G). As a critical member of the UPR, *XBP1* regulates the terminal
376 differentiation of B cells into plasma B cells[40] and controls downstream genes involved in
377 protein synthesis (Figure S9C). Hypoxia can induce *XBP1* mRNA expression and activate its
378 mRNA splicing[41], and a positive correlation between the hypoxia score and the expression of
379 *XBP1* was observed in plasma B cells (Figure 4H). Taken together, these results demonstrated that
380 high-altitude mountaineering induced the activation of the UPR in plasma B cells, which may
381 contribute to the enhancement of humoral immunity in mountain climbers.
382
383 **Metabolic reprogramming of circulating immune cells in mountain climbers**
384 Pathway enrichment analysis revealed a reduction in the levels of oxidative phosphorylation in
385 $CCL3^+$ $CD14^+$ Monos and pDCs during mountaineering (Figure S5C and S6A). Considering the
386 profound impact of metabolic programs on immune cell function[18], an analysis of metabolic
387 features centered on oxidative phosphorylation and the glycolysis pathway across different cell
388 types was performed. The expression level of oxidative phosphorylation increased on D4 but
389 decreased significantly on D9, D11 and D16, especially in monocytes (Figure 5A and 5B). In

390 contrast, the expression level of glycolysis decreased on D4 and D9 but significantly increased on
391 D11 and D16 (Figure 5A). This change was consistent with the observed variation in the hypoxia
392 pathway, which was initially suppressed and subsequently activated (Figure 2D and S10A). A
393 positive correlation between the hypoxia score and glycolysis score was observed in different
394 immune cell subgroups (Figure S11A and S11B), suggesting that hypoxia may be a key factor in
395 regulating the metabolic program of immune cells during mountaineering. The expression of
396 mitochondrial electron transport chain (ETC) subunits was downregulated. For instance, the
397 expression of *ATP5F1E* (ATP synthase complex) was significantly downregulated during
398 mountaineering in CCL3^{+} CD14^{+} Monos, FCN1^{+} CD14^{+} Monos, C1^{+} CD16^{+} Monos and cDC2s
399 (Figure 5C). Decreased expression levels of *COX4I1*, *COX7A2*, *COX5B* and *COX7C* (complex IV)
400 were observed in IFN^{+} CD16^{+} Monos (Figure 5D). It was evident that the activity of the
401 mitochondrial ETC decreased under high-altitude hypoxic conditions. HIF is widely recognized as
402 the primary regulator of metabolic adaptation to hypoxia and can drive a switch from oxidative to
403 glycolytic metabolism during hypoxia[42]. Interestingly, significantly upregulated *HIF1A*
404 expression was observed on D11 and D16 in most subgroups, except for pDCs (Figure 2H and
405 S10A). Moreover, the expression of *LDHA* (lactate dehydrogenase A) and *GAPDH*
406 (glyceraldehyde 3-phosphate dehydrogenase) was significantly elevated during mountaineering in
407 CD8^{+} Tems and plasma B cells, respectively (Figure 5E). *LDHA* encodes a key enzyme in
408 glycolysis that facilitates the conversion of pyruvate to lactate. *GAPDH* is an essential component
409 of glycolysis that catalyzes the conversion of glyceraldehyde-3-phosphate to 1,3-
410 bisphosphoglycerate[43]. We also observed upregulated expression of the glucose transporter
411 *SLC2A3* on D11 and D16(Figure 5E); this gene facilitates cellular glucose uptake to support the
412 glycolytic pathway[44]. Taken together, these observations suggested that the circulating immune
413 cells of mountain climbers may undergo metabolic reprogramming.
414
415 Cell energy sensors also play important roles in the metabolic regulation of immune cells[15].
416 AMP-activated protein kinase (AMPK) serves as the main regulator of intracellular energy
417 homeostasis and can be activated by various stimuli, including cellular stress and physical
418 activity[45]. The activity of the AMPK-related pathway 'CAMKK AMPK Signaling Cascade'
419 was significantly increased on D4 and D9, particularly in monocytes; however, it decreased on

420 D11 and D16 (Figure 5F and S10B). The expression of the AMPK subunits *PRKAB1* and
421 *PRKAB2*, as well as the upstream kinase *CAMMK2*, was upregulated on D4 and D9 in CCL3$^+$
422 CD14$^+$ Monos, FCN1$^+$ CD14$^+$ Monos, cytotoxic CD8$^+$ T cells and γδT cells (Figure S10C). In
423 addition, the expression level of *PRKAA1* was also significantly upregulated on D4 and D9 in
424 cytotoxic CD8$^+$ T cells (Figure S10C). *PRKAA1* is crucial for the proliferation and differentiation
425 of cytotoxic T lymphocytes[46]. Activation of the AMPK pathway can not only promote the
426 metabolic adaptation of immune cells but also exert a wide variety of immunoregulatory
427 effects[47]. For example, the AMPK pathway exerts inhibitory effects on the inflammatory
428 response of macrophages and DCs while promoting T cell effector function[48, 49]. In our study,
429 we observed that during the period of acclimation, when the AMPK-related pathway was activated,
430 the inflammatory response in monocytes and cDC2s was suppressed, and the immune effector
431 process of cytotoxic CD8$^+$ T cells was upregulated (Figure 5G). In contrast, the activity of the
432 AMPK-related pathway decreased during extreme altitude mountaineering, whereas the activity of
433 the hypoxia pathway increased, accompanied by the activation of inflammatory responses in
434 monocytes and cDC2s and a decrease in the immune effector process in cytotoxic CD8$^+$ T cells
435 (Figure 5G). Overall, our findings suggested that the dynamic activation of the AMPK and
436 hypoxia pathways induced by high-altitude mountaineering may play crucial roles in regulating
437 the metabolism and function of immune cells.
438
439 **The defense of circulating immune cells against oxidative stress in mountain climbers**
440 Previous findings have indicated that exercise at high altitudes increases the generation of
441 ROS[17]. When ROS production exceeds the load capacity of the antioxidant system, it can lead
442 to oxidative stress. The pathway scores for 'Cellular Response to Reactive Oxygen Species' and
443 'Cellular Response to Oxidative Stress' were calculated for each immune subgroup, and we found
444 that the scores decreased on D4 and D9 and then increased on D11 and D16 in most subgroups, in
445 addition to pDCs and several B cell subgroups (Figure 6A). A positive correlation between the
446 hypoxia score and oxidative stress score was observed for circulating immune cells (Figure 6B).
447 These findings indicated that circulating immune cells manifested distinct reactions to oxidative
448 stress during high-altitude mountaineering.
449

450 Moreover, cells are equipped with an antioxidant system that scavenges excess ROS to reduce
451 oxidative damage[50]. We next calculated the pathway scores for 'Cellular Oxidant Detoxification'
452 in different immune subsets and observed increased scores in T and NK cells on D4, whereas the
453 scores were generally lower in most subgroups on D9, D11 and D16 (Figure 6A). Notably, the
454 oxidative detoxification scores were greater on D11 and D16 in monocytes and plasma B cells
455 (Figure 6A). The expression of multiple antioxidant genes in different mountaineering stages,
456 including *SOD2*, *NFE2L2*, *SOD1*, *GPX4* and *TXNRD1*, was significantly upregulated on D11 and
457 D16 (Figure 6C). Among them, *SOD2* and *NFE2L2* levels were significantly increased in
458 monocytes and DCs but not in pDCs (Figure 6D). The SOD2 enzyme is specifically localized to
459 the mitochondrial matrix at the main site of superoxide production and catalyzes the reaction of
460 superoxide to less reactive hydrogen peroxide[51]. *NFE2L2* (also known as *NRF2*) serves as a
461 central regulator that responds to oxidative stress by controlling a battery of defensive genes
462 encoding antioxidant and detoxification enzymes[52]. In addition, we observed that the expression
463 of *PRDX4* and *TXN* was significantly elevated in plasma B cells during mountaineering (Figure
464 4F). In contrast, markedly decreased expression of *SOD1*, *TXN*, *PRDX5* and *PRDX6* was observed
465 in pDCs (Figure S6B). *TXN* and *PRDXs* are major members of the thioredoxin system, which is
466 one of the central antioxidant systems and plays a vital role in maintaining the intracellular ROS
467 balance[53]. In particular, *PRDX4*, a typical endoplasmic reticulum (ER)-resident antioxidant that
468 scavenges excess H_2O_2, is essential for the correct folding of proteins[54]. Generally, when the
469 level of oxidative stress increased on D11 and D16, monocytes and plasma B cells exhibited
470 enhanced oxidative detoxification ability, while pDCs and most T and NK cells exhibited
471 decreased oxidative detoxification ability. These results highlighted the importance of the
472 enhanced antioxidant capacity of circulating immune cells to defend against elevated oxidative
473 stress and further maintain their immune functions.
474
475 **Plasma metabolic changes in mountain climbers**
476 Metabolic reprogramming in immune cells is observed during mountaineering, and metabolic
477 changes in immune cells may be localized, but if they occur across multiple cells or tissues, such
478 changes can result in systemic metabolic alterations[18]. To explore the plasma metabolic
479 alterations in mountain climbers during mountaineering, we conducted VIP and c-means

480 clustering analysis. According to the VIP scores, the levels of some metabolites, including 3-
481 methyloxindole, N-acetyl-L-aspartic acid, asparagine, glycine and palmitoylcarnitine, increased
482 during mountaineering, while the levels of other metabolites, such as glucose and piperine,
483 decreased (Figure 7A). Four change patterns were identified in different periods of
484 mountaineering: cluster 1 contained analytes whose levels were sharply decreased on D4 and D9,
485 followed by analytes whose levels were increased on D11 and decreased on D16; cluster 4
486 exhibited the opposite trend (Figure 7B); the analytes in cluster 2 exhibited a sharp decrease on D4
487 and subsequently remained at a low level; and the analytes in cluster 3 showed a pattern of a
488 gradually decreasing trend (Figure 7B). The differentially abundant metabolites were mainly
489 distributed in cluster 1 and cluster 4, whereas differential lipids exhibited a predominant
490 distribution in cluster 2 and cluster 3 (Figure 7B).
491
492 The analytes in cluster 1 were mainly enriched in serine and glycine metabolism, representative
493 metabolites that included glycine, serine and methionine (Figure 7C and S12A). The levels of
494 serine and glycine decreased on D4 and D9, followed by an increase on D11 and D16 (Figure 7D).
495 The concentration of plasma glycine is regulated by glucagon, which stimulates the degradation of
496 glycine, and glucagon deficiency elevates the level of glycine[55]. Furthermore, intense physical
497 activity may result in increased muscle protein breakdown and the subsequent release of amino
498 acids into the bloodstream[56], potentially resulting in increased glycine levels. The increased
499 availability of glycine can be utilized for the synthesis of serine and glutathione. The role of
500 glutathione as a vital antioxidant lies in its ability to reduce cellular damage induced by oxidative
501 stress[57]. The analytes in cluster 2 were not enriched in metabolic pathways, and those in cluster
502 3 were mainly involved in tryptophan metabolism (Figure S12B).
503
504 The analytes in cluster 4 were enriched in glutamine metabolism, and representative metabolites
505 included glutamine, N-acetyl-L-aspartic acid, alanine and gamma-aminobutyric acid (GABA)
506 (Figure 7C, 7D and S12A). Glutamine is the most abundant circulating amino acid in plasma, as it
507 is a carbon source second only to glucose, which can generate 2-oxoglutarate through
508 glutaminolysis[58]. Consistently, the levels of citrate cycle (TCA cycle)-related substances,
509 including 2-oxoglutarate and isocitric acid, increased during mountaineering (Figure S12C). It has

510 been suggested that mountain climbers may rely on glutamine as an important anaplerotic
511 substrate to complete the TCA cycle during mountaineering, consistent with previous studies
512 showing that high altitude-exposed individuals presented increased plasma glutamine[59].
513 Importantly, glutamine can actively improve immune function, and glutamine supplementation
514 may reduce the incidence of infections reported by marathon runners[60]. In addition, GABA, a
515 neurotransmitter, has a variety of biological functions, including antifatigue and immune
516 regulation activities[61].
517
518 Analytes in cluster 4 were also involved the metabolism of selenocompounds, from which
519 selenomethionine (Se-Met) (Figure 7C and S12C), a natural organic selenium, is a key metabolite.
520 As the main source of selenium in humans, Se-Met has been shown to have important antioxidant
521 properties involving the formation of antioxidant enzymes[62]. Se-Met increased on D4 and D9
522 but significantly decreased on D11 (Figure 7E). The decreased level of Se-Met may be related to
523 the increased oxidative stress response observed in immune cells, as a significant positive
524 correlation between selenocompound metabolism and oxidative stress in circulating immune cells
525 was observed (Figure 7F). Intriguingly, we observed a similar variation trend in omega-3
526 polyunsaturated fatty acids (n-3 PUFAs), alpha-linolenic acid, docosahexaenoic acid,
527 docosapentaenoic acid and eicosapentaenoic acid (Figure 7E). PUFAs are vulnerable to ROS
528 attack due to their structural instability, resulting in a marked increase in the end-product
529 malondialdehyde (MDA), which is a biomarker of oxidative stress[63].
530
531 In addition, fatty acid oxidation may be activated on D11 and D16, as reflected by the
532 accumulation of acylcarnitines and medium- to long-chain fatty acids (Figure S12D).
533 Acylcarnitine is an intermediate product of fatty acid oxidation, and the heart is considered the
534 main contributor to the increased abundance of long-chain acylcarnitines in plasma[64], such as
535 palmitoylcarnitine and stearoylcarnitine (Figure S12D). These changes were concomitant with the
536 accumulation of 3-hydroxybutyric acid, the main ketone body in the blood (Figure S12E). Ketone
537 bodies are predominantly produced from fatty acid β-oxidation-derived acetyl-CoA in the liver
538 and serve as key contributors to energy metabolism in the context of energy-depleted states[65].
539 These observations suggested that the utilization of fatty acids might be enhanced during extreme

540 altitude mountaineering.

541

542 Clusters 2 and 3 mainly contained complex lipids, such as triacylglycerol (TAG),
543 lysophosphatidylcholine (LPC), phosphatidylethanolamine (PE), phosphatidylcholine (PC),
544 phosphatidylinositol (PI), lysophosphatidylethanolamine (LPE), ceramide (CER) and
545 sphingomyelin (SM) (Figure 7B and 7G). The role of lipids is critical for cell
546 structure, intracellular and extracellular signaling and energy storage. The levels of TAG, LPC, PE
547 and PC decreased significantly during mountaineering (Figure 7H). TAG molecules represent the
548 major form of fatty acid storage within cells, and in the plasma, prolonged exercise has been
549 reported to accelerate plasma TAG clearance[66]. LPC can activate a variety of signaling
550 pathways in monocytes/macrophages through G protein-coupled receptors and Toll-like receptors,
551 further increasing the production of proinflammatory cytokines, whose downregulated expression
552 is considered associated with worse health status[67]. PE and PC are the most abundant
553 phospholipids in mammalian cell membranes and play crucial roles in regulating lipid metabolism
554 and maintaining membrane protein stability[68]. The progressive decrease in plasma PE levels
555 during mountaineering may be regarded as a potentially positive change[69]. The levels of PI and
556 LPE were significantly decreased on D4 and D9 and then gradually recovered, while the levels of
557 CER and SM were significantly decreased on D4 and D9 (Figure 7H). CER is the precursor of
558 most SM. The plasma concentration of SM is altered in various metabolic disorders, serving as a
559 valuable indicator for prognosis and diagnosis[70]. Overall, the observed decrease in lipid levels
560 may reflect lipid metabolism disorders during mountaineering.

561

562 **DISCUSSION**

563 Extreme adventure sports, such as high-altitude mountaineering, have become increasingly
564 popular. High-altitude mountaineering involves exposure to a hypobaric hypoxic environment,
565 leading to a series of physiological, metabolic and immunological changes. Circulating immune
566 cells, including monocytes, DCs, T cells, NK cells and B cells, function as “sentinel tissue” to
567 monitor the body’s response[71]. Previous studies have proposed peripheral blood lymphocytes as
568 biosensors for whole-body responses to high altitudes[16]. However, few studies have
569 investigated the response profiles of circulating immune cells during mountaineering. We

570 identified and characterized the immune response and metabolic changes during high-altitude
571 mountaineering. Importantly, the mountaineering plan consisted of two stages (the first being the
572 period of acclimatization, and the second being the period of extreme altitude mountaineering).
573 Sampling at multiple time points enabled a more comprehensive understanding of the immune
574 response alterations and adaptation characteristics of mountain climbers in different periods.
575
576 Research in the field of exercise immunology has demonstrated that physical activity can
577 induce significant alterations in the immune response, contingent upon exercise intensity, duration,
578 and type[72]. Moderate-intensity exercise is acknowledged to confer a multitude of
579 immunological benefits, including augmented immunosurveillance, diminished systemic
580 inflammation levels, and heightened lymphocyte concentrations, whereas prolonged or high-
581 intensity exercise is associated with immune dysfunction, elevated inflammation levels and
582 heightened susceptibility to infectious disease[7, 8]. Our analysis revealed that high-altitude
583 mountaineering induced intricate and dynamic immune alterations in mountain climbers. Climbers
584 exhibited distinct immune alterations in the two stages of mountaineering. During the acclimation
585 period, for myeloid cells, we observed the significant suppression of the inflammatory response in
586 monocytes and cDCs. The immunosuppressive phenotype of $CCL3^+$ $CD14^+$ Monos was
587 subsequently characterized by notable the upregulation of *S100A8* and *S100A9* expression and
588 marked downregulation of the expression of multiple inflammatory genes on D4 and D9. The
589 upregulation of *S100A8* expression has been documented in individuals acutely exposed to high
590 altitudes[73]. For lymphocytes, the proportions of cytotoxic $CD8^+$ T, γδT and $CD16^+$ NK cells
591 were significantly increased on D4, and the expression of effector process-related genes was
592 significantly upregulated on D4. Notably, AMPK-associated pathways were also activated on D4
593 and D9 in monocytes, cDC2s, cytotoxic $CD8^+$ T cells and γδT cells.
594
595 As one of the central regulators of cellular metabolism, AMPK plays a critical role in
596 orchestrating cellular metabolic reprogramming. Under conditions of low energy availability,
597 AMPK phosphorylates downstream targets to enhance adenosine triphosphate (ATP) production
598 while reducing ATP consumption[45]. Previous studies have demonstrated that exercise-induced
599 activation of AMPK can confer a wide range of health benefits, making it an attractive target for

600 the treatment of immune-related diseases[47, 74]. In myeloid cells, AMPK exerts inhibitory
601 effects on inflammatory responses[48], highlighting the intricate interplay between inflammation
602 and AMPK signaling. In T cells, AMPK plays a pivotal role in regulating T cell-mediated
603 adaptive immunity[49]. This finding aligned with our observation that during the acclimation
604 period, when the AMPK-related pathway was activated, there was a concomitant suppression of
605 the inflammatory response in monocytes and cDCs and an increase in effector process scores for
606 cytotoxic $CD8^+$ T cells.
607
608 During extreme high-altitude mountaineering, monocyte- and cDC-mediated inflammatory
609 responses were significantly activated on D11 and D16, with increased expression of *IL1B*, *TNF*
610 and *NFκB1*, in line with the observed increase in CRP levels during trekking in the Himalayas[5].
611 Proinflammatory *IL1B* expression has been reported to be correlated with worsening symptoms of
612 acute mountain sickness (AMS)[75], and the exacerbation of the inflammatory response in high-
613 altitude hypoxic environments may contribute to the pathogenesis of diseases, such as chronic
614 obstructive pulmonary disease or chronic obstructive sleep apnea[76]. Compared to those on D1,
615 the proportions of cytotoxic $CD8^+$ T, γδT and $CD16^+$ NK cells on D16 were significantly lower,
616 accompanied by the downregulated expression of genes associated with immune effects, including
617 *GZMA*, *GZMK*, *GZMH*, *NKG7*, *KLRD1*, *CD160* and *CX3CR1*. These findings are consistent with
618 the observed decrease in the percentage of cytotoxic T cells following a marathon[20]. The
619 impairment of T cell-mediated function at extreme altitudes might disrupt immune homeostasis
620 and increase the risk of infectious disease. These observations may be attributed to the increased
621 intensity of physical activity during extreme altitude mountaineering (D11 and D16), which could
622 further exacerbate the degree of hypoxia. Importantly, the activity of the hypoxia pathway was
623 significantly activated on D11 and D16 in most immune cells.
624
625 The effect of hypoxia on the inflammatory response has been widely reported in studies of
626 high-altitude environments[24]. On the one hand, hypoxia-induced *HIF1A* can upregulate the
627 expression of *NF-κB*; on the other hand, hypoxia promotes the release of *NF-κB* and its
628 translocation to the nucleus by activating the IKKβ pathway, further upregulating the transcription
629 of inflammatory genes[77]. Among T and NK cells, the upregulation of the immunoregulatory

630 gene *TGFB1* was observed in cytotoxic CD8$^+$ T and γδT cells on D11 and D16. Hypoxia-induced
631 *TGFB1* may exert inhibitory effects on the expression of *TBX21* and *EOMES* in T cells[35, 78].
632 Similarly, *TGFB1* also downregulated the expression of *TBX21* in NK cells[79]. Within plasma B
633 cells, hypoxia may promote the activity of *XBP1*[41], which controls the downstream genes
634 involved in protein synthesis. Notably, the activity of the hypoxia pathway and the expression of
635 *HIF1*A were significantly increased in most cell types during extreme altitude mountaineering,
636 while decreased hypoxia scores and low *HIF1A* expression were observed in functionally
637 impaired cells, such as pDCs, confirming the key role of hypoxia in regulating the immune
638 response of mountain climbers.
639
640 Furthermore, another intriguing finding in our study is the adaptation characteristics of
641 circulating immune cells during extreme altitude mountaineering. Considering the exposure to
642 high-altitude hypoxic conditions coupled with intense physical activity, the energy and metabolic
643 homeostasis of mountain climbers may be challenged substantially. We observed a decrease in
644 oxidative phosphorylation activity and an increase in glycolytic activity on D11 and D16 in most
645 immune cells. Previous studies have reported that climbers experience attenuated mitochondrial
646 function after exposure to high altitudes[16, 80]; these findings imply that the functionality of
647 mitochondria might be constrained under high-altitude conditions. Notably, the expression of the
648 glycolysis-related genes *LDHA*, *GAPDH* and *SLC2A3* was significantly enhanced on D11 and
649 D16 in CD8$^+$ Tems and plasma B cells. HIF is known to play an important role in hypoxia-induced
650 reprogramming, and increased *HIF1A* expression was observed on D11 and D16 in most immune
651 cells. Moreover, we observed increased pathway activity in most subgroups in response to ROS
652 and oxidative stress on D11 and D16, which was consistent with previous studies showing that
653 exercise at high altitudes increased the levels of oxidative stress[13]. In the context of increased
654 oxidative stress on D11 and D16, monocytes and plasma B cells showed increased expression of
655 antioxidant-related genes (*NFE2L2*, *SOD2*, *PRDX4* and *TXN*) on D11 and D16. *NFE2L2* is the
656 major transcription regulator in the cellular response to oxidative stress[52]. An increase in SOD
657 activity is considered a crucial adaptive mechanism for coping with hypoxic conditions at high
658 altitudes to reduce oxidative damage[81].
659

660 Finally, the high-resolution analysis of plasma analytes revealed numerous molecules affected
661 by high-altitude mountaineering, and these metabolic processes were involved in energy
662 metabolism (amino acid and fatty acid metabolism) and oxidative stress (selenocompound
663 metabolism), suggesting the crucial involvement of metabolites in metabolic adaptation in
664 climbers. In high-altitude hypoxic environments, mountain climbers are in a low-sugar state,
665 which may improve their energy supply by promoting glutamine metabolism and fatty acid
666 metabolism. Interplay among metabolism, oxidative stress and immunity was observed, reflected
667 in selenocompound metabolism, and a positive correlation between selenocompound metabolism
668 and oxidative stress was also observed in circulating immune cells.
669
670 In conclusion, the results of our study provide a multi-omics profile of the response to high-
671 altitude mountaineering. We used a single-cell transcriptome to analyze the circulating immune
672 profile of climbers, revealed distinct immune responses during two stages of mountaineering, and
673 explored the adaptive characteristics of circulating immune cells during extreme altitude
674 mountaineering. The enhanced expression of glycolysis and antioxidant genes was shown to play
675 a crucial role in supporting the functionality of immune cells. Conversely, decreased expression of
676 those genes was observed in pDCs with impaired immune function. Furthermore, the energy status
677 of mountain climbers can potentially be promoted through the enhancement of glutamine
678 metabolism and fatty acid metabolism.
679
680 **Data availability**
681 The scRNA-seq data generated by this study were deposited at the China National GeneBank
682 (CNGB) Sequence Archive (https://db.cngb.org/cnsa/) under accession nos. Other relevant data
683 are available from the corresponding author upon reasonable request.
684
685 **Code availability**
686 R codes and other custom scripts are available upon reasonable request.
687
688 **Acknowledgements**
689 We sincerely thank the eleven mountain climbers who enthusiastically participated in this

mountaineering expedition. This work was supported by the Guangzhou Basic and Applied Basic Research Program (202201010189) and the National Key R&D Program of China (2022YFC3400400). We would also like to acknowledge the support from the Chinese National Gene Bank.

Author contributions

Experimental strategy and design: J.W., X.J., C.Y.L., J.C., L.Q.L., J.H.Y.

Laboratory experiments: Y.W., X.M.L., Y.T.H., Y.Y., Y.L.H., C.L., G.X.H., H.R.T., H.H.L., Y.Z., G.D.Z.

Statistical analyses: S.C.Y., J.Z.L., Z.L.H., X.W., Y.L., W.K.W., Y.H.Z., C.W.

Manuscript writing: J.H.Y., J.Z.L., S.C.Y.

Manuscript editing: J.H.Y., J.Z.L., W.W.Z., R.Q.L.,

All authors critically revised the manuscript for important intellectual content and gave final approval for the version to be published. All authors agree to be accountable for all aspects of the work in ensuring that questions related to the accuracy or integrity of any part of the work are appropriately investigated and resolved.

720 **METHODS**

721 **Sample collection and ethics statement**

722 This study was performed during an expedition to summit the Muztagh Ata peak (7,546 m), and
723 eleven healthy volunteers residing at low altitudes (< 300 m) were recruited to participate in the
724 expedition. None of the individuals had known chronic diseases, such as cardiovascular or
725 respiratory system disorders. During mountaineering, we monitored the dynamic changes in 10
726 physiological parameters (e.g., routine blood tests, SpO_2, HR, LLS and body composition) of
727 climbers using professional equipment. To investigate alterations in metabolism and the immune
728 response during high-altitude mountaineering, 55 blood samples were collected from climbers at
729 five distinct time points. The research protocol received approval from BGI's institutional review
730 board of bioethics and biosafety, and written informed consent was obtained from each individual
731 participating in the mountaineering expedition.

732

733 **Protocol for the mountaineering expedition**

734 For the mountaineering itinerary, participants reached 1,289 m on the first day (D1), and the
735 mountaineering expedition was divided into two phases: an initial acclimatization period (D2-D8)
736 followed by an extreme altitude mountaineering period (D9-D15). The participants embarked on a
737 trek to reach 3,200 m and subsequently arrived at the base camp (4,400 m) on D3. From there,
738 acclimatization to high altitudes was carried out at the base camp. During this period, the
739 participants ascended to Camp 1 (5,500 m) on D5, followed by a two-day rest at base camp before
740 proceeding to Camp 2 (6,300 m) on D9. Finally, the participants undertook a four-day consecutive
741 ascent from base camp to the summit (7,546 m). Before reaching the summit, five out of the
742 eleven individuals utilized supplemental oxygen for a duration of time on D15. On D16, the
743 participants returned 1,289 m. During the expedition, 55 blood samples at five different time
744 points (D1, D4, D9, D11 and D16) were collected. Fasting blood samples for each participant
745 were collected at 9:00 a.m.; the fifth sampling was performed before dinner due to itinerary
746 constraints. No medications (including acetazolamide) were taken by the participants during the
747 expedition. According to the LLS, none of the eleven participants suffered from severe acute
748 mountain sickness. For additional details, see Supplementary Table 1.

749

750 **Plasma and peripheral blood mononuclear cells (PBMCs) separation**

751 Plasma and PBMC isolation were conducted with the following protocols. The whole blood of the
752 mountain climbers was collected in 5mL EDTA anticoagulant tubes. Briefly, 5 mL of whole blood
753 was centrifuged at 940×g for 10 min, after which the upper plasma layer was transferred to a 15-
754 mL centrifuge tube, collected after centrifugation at 2,600×g for 10 min, aliquoted, and stored at -
755 80 °C. The lower immune cells were diluted with 1x phosphate-buffered saline (PBS)
756 supplemented with 2% bovine serum albumin (BSA) and transferred to SepMate^{TM}–50 tubes.
757 After centrifugation at 1200×g for 10 min, the PBMC layer was poured into a new centrifuge tube.
758 The cells were washed twice with 3 mL of 1× PBS containing 2% fetal bovine serum (FBS) and
759 centrifuged at 300×g for 8 min. The supernatant was discarded, and the PBMC pellet was
760 resuspended in FBS supplemented with 10% dimethylsulfoxide (DMSO). Afterwards, the frozen
761 tubes were transported on dry ice to be stored in liquid nitrogen at the end of the expedition.

762

763 **Preparation of single-cell suspensions**

764 To thaw the frozen PBMCs, the cells were placed in a 37 °C water bath for 2 min, after which the
765 cells were gently poured into a 15-mL centrifuge tube. The thawed cells were resuspended in 10
766 mL of preheated 1× PBS supplemented with 10% FBS at 37 °C and mixed gently. After
767 centrifugation at 500×g for 5 min at room temperature, the supernatant was removed, and the cell
768 pellet was resuspended in 2 mL of PBS supplemented with 0.04% BSA. The cells were strained
769 through a 40-μm cell strainer, and the filtered cells were collected and then resuspended at a
770 concentration of 800-1,500 cells/μL. The cell suspensions were maintained on ice for sequencing.

771

772 **Sequencing library construction**

773 The sequencing libraries were constructed according to the instructions of the DNA Nanoball
774 (DNB) elab C4 scRNA Preparation Kit (MGI). The prepared single-cell suspension, the barcode
775 mRNA capture beads, and the droplet generation oil were loaded into the corresponding reservoirs
776 on a microfluidic chip for droplet generation. The cells were lysed, and the released mRNA was
777 captured and barcoded in the droplets. Following reverse transcription, complementary DNA
778 (cDNA) was generated and amplified. The amplified cDNA was quantified using a BioAnalyzer
779 High Sensitivity Chip (Agilent) and subsequently fragmented to 400-600 bp with NEBNext

780 dsDNA Fragmentase. The cDNA and oligo library construction steps were performed as follows.
781 The libraries were made of DNBs and sequenced on an ultrahigh-throughput DNBSEQ-T1
782 sequencer at the CNGB. cDNA libraries were generated using the following read lengths: 41-bp
783 read 1 (containing a 20-bp cell barcode and a 10-bp unique molecular identifier (UMI)), 100-bp
784 read 2, and a 10-bp sample index. The following oligo libraries were used: 26-bp read 1, 42-bp
785 read 2, and 10-bp sample index.
786
787 **Single-cell RNA-seq data processing**
788 Sequencing data were processed using the Open Source Pipeline (https://github.com/MGI-tech-
789 bioinformatics/DNBelab_C_Series_HT_scRNA-analysis-software). First, bead barcodes and UMI
790 sequences were extracted using the parsing function in PISA (https://github.com/MGI-tech-
791 bioinformatics/DNBelab_C_Series_HT_scRNA-analysis-software/software/PISA). Reads with
792 incorrect barcodes were excluded based on the use of a barcode whitelist. The scRNA-seq data
793 were then aligned to the GRCh38 (hg38) reference genome using STAR[82]. Finally, gene
794 expression levels in cells were assessed using PISA, and gene-cell matrices were created for each
795 library.
796
797 Then, we used the R package Seurat (version 4.4.0) to apply preliminary counts to downstream
798 data analysis, including quality control, normalization, feature selection, dimensionality reduction,
799 unsupervised clustering, and visualization[83]. First, cells with more than 10% mitochondrial
800 genes, more than 1% erythrocyte genes, and less than 200 or more than 6,000 genes were
801 excluded. Then, for each library, DoubletFinder (version 2.0.3) was used to remove doublets[84].
802 The top 5% of cells most similar to the "pseudo-doublet" were excluded. Finally, genes expressed
803 in fewer than three cells, as well as mitochondrial genes, noncoding RNA genes, and ribosomal
804 genes were filtered. In addition, a portion of the cells were clustered together by red blood cells
805 contamination with highly expressed red blood cell genes, and we removed the red blood cell
806 clusters to eliminate the effect on clustering. Subsequently, the "NormalizeData" function was
807 used to convert the data into logarithmic space, and the "FindVariableGene" function was used to
808 find the top 2,000 variable genes in the dataset. Then, "ScaleData" was used to remove unwanted
809 variations due to differences in sequencing depth. The first 20 principal components (PCs) were

810 computed using RunPCA. Finally, Harmony (version 1.1.0) was used to correct for batch effects
811 of different library.
812
813 **Unsupervised clustering and subclustering**
814 The Louvain algorithm was used as a modular optimization technique to set the granularity of the
815 clusters at a resolution of 0.75. The nonlinear dimensionality reduction technique "UMAP" was
816 used to visualize the clusters in two-dimensional space. Cellular identity was determined by
817 identifying differentially expressed genes (DEGs) for each cluster using the "FindALLMarkers"
818 function with default parameters and comparing those genes to known cell type-specific genes.
819 The clusters were annotated based on typical marker expression, and 15 cell subpopulations were
820 identified. After scaling, myeloid, $CD4^+$ T, $CD8^+$ T, NK, and B cell clusters were extracted as
821 separate Seurat objects; the principal components were identified, each subset was clustered at a
822 unique resolution using the Louvain algorithm, and the clusters were annotated based on
823 dimensionality and gene expression associated with the phenotypes of the typical subsets
824 described above.
825
826 **DEGs and GO enrichment analysis**
827 To search for DEGs in each cell subgroup during mountaineering, we used the "FindMarkers"
828 function (Seurat). For each cell subgroup, we computed the fold change in mean gene expression
829 levels between D1 and subsequent time points, and the p value was calculated utilizing the
830 Wilcoxon rank sum test. To annotate the functions of these DEGs, we performed GO pathway
831 enrichment analysis by using the clusterProfiler package (version 4.10.0) in R (OrgDb =
832 org.Hs.eg.db, pvalueCutoff = 0.05, qvalueCutoff = 0.05, pAdjustMethod = "BH") to enrich the
833 DEGs in GO terms[85]. For DEG details, see Supplementary Tables 4, 5 and 6.
834
835 **Module scores for feature gene set expression**
836 To assess the dynamic changes in biological processes mediated by immune cell subsets, we
837 employed the "AddModuleScore" (Seurat) function to assess the scores for the gene sets. Briefly,
838 the score for each cell was defined as the average expression of the featured gene set minus the
839 average expression of the corresponding control feature gene set. The referenced gene sets are

840 listed in Supplementary Table 7 and were collected from the Molecular Signatures Database
841 (MSigDB)[86]. The Wilcoxon rank-sum test was used to evaluate the statistical significance of
842 differences between D1 and subsequent time points.
843
844 **Gene regulatory network analysis based on SCENIC**
845 To predict the potential transcriptional regulatory networks in different immune cell subgroups,
846 we used pySCENIC (version 0.12.1). Initially, we employed GRNBoost to infer all potential
847 targets of transcription factors. Subsequently, the output coexpression module was utilized in
848 conjunction with the cisTarget database to identify putative regulators. The regulon areas under
849 the curve per cell (AUCell) module of pySCENIC was used to analyze regulator activity, and
850 active regulators were identified using the default thresholds[23]. The differentially expressed
851 regulators were identified using the R package limma (version 3.50.0) with the following
852 parameters: adjusted $p \leqslant 0.05$ and $|\text{logFoldChange}| \geqslant 0.4$. For regulator details, see
853 Supplementary Table 8.
854
855 **Target metabolite quantification by HM Meta Assays**
856 The HM Meta Assay (BGI, Shenzhen, China) was utilized for quantifying metabolites. This assay
857 covers a wide range of chemical classes, including bile acids, amino acids, fatty acids, carboxylic
858 acids, hydroxyl acids, phenolic acids and indoles, by measuring 700 compounds. Calibration
859 curves were generated using serial dilutions of metabolite standards. In 96-well plates, 20-μL
860 aliquots of either standards or plasma samples were mixed with 120 μL of internal standard
861 solution (methanol-diluted metabolite internal standards). The plates were then stored at -20 °C
862 for 20 min, followed by centrifugation at 4,000 × g and 4 °C for 30 min. The supernatants (30 μL)
863 were transferred to new plates for derivatization with freshly prepared reagents (10 μL), which
864 included a mixture of 200 mM 3-NPH in 75% aqueous methanol and 96 mM EDC-6% pyridine in
865 methanol. Derivatization took place at 30 °C for one hour. Prior to LC–MS analysis, the samples
866 were diluted with ice-cold 50% methanol and then transferred to new plates containing 135 μL of
867 the supernatant.
868
869 A Waters ACQUITY UPLC instrument coupled to a SCIEX QTRAP 6500 PLUS mass

870 spectrometer equipped with an ESI source controlled by Analyst software was used for UPLC-
871 MRM analysis. Chromatographic separation was performed on a Waters ACQUITY BEH C18
872 column (1.7 μm particle size; dimensions: 100 mm × 2.1 mm). Both positive and negative ion
873 modes were employed during instrument operation. Ultimately, HMQUANT software (BGI,
874 Shenzhen, China) was used for the absolute quantification of metabolites.
875
876 **Target lipid quantification by HM lipid assays**
877 Lipid measurement was conducted using the HM Lipid Assay (BGI, Shenzhen, China). This assay
878 covers a wide range of lipid subclasses and quantifies 1600 lipid molecules, including 18 lipid
879 classes: SM, CER, cholesterol ester (CE), monoacylglycerol (MAG), diacylglycerol (DAG), TAG,
880 lysophosphatidic acid (LPA), phosphatidic acid (PA), LPC, PC, LPE, PE,
881 lysophosphatidylinositol (LPI), PI, lysophosphatidylglycerol (LPG), phosphatidylglycerol (PG),
882 lysophosphatidylserine (LPS) and phosphatidylserine (PS). Calibration curves were generated
883 using serial dilutions of lipid standards. In 96-well plates, aliquots of either standards or plasma
884 samples were mixed with internal standard solution (precooled isopropanol with SPLASH internal
885 standards, avanti) (20 μL each). The plates were then stored at -20 °C for 20 min before being
886 centrifuged at 4,000 × g and 4 °C for 30 min. Supernatants containing lipids were transferred to
887 new plates for LC-MS analysis in negative mode, while a portion of the supernatants was diluted
888 into methanol for LC-MS analysis in positive mode.
889
890 UPLC-MS/MS analysis was performed on a Waters ACQUITY UPLC coupled to a SCIEX
891 QTRAP5500 PLUS mass spectrometer equipped with an ESI source controlled by Analyst
892 software. Chromatographic separation was performed on a Waters ACQUITY CSH C18 column
893 (1.7 μm, 100 mm × 2.1 mm). SM, CE, Cer, TAG, DAG, and MAG were quantified in positive
894 mode, whereas the phospholipids and lysophospholipids were quantified in negative mode
895 utilizing the scheduled MRM settings. HMQUANT software (BGI, Shenzhen, China)
896 incorporating isotope correction via the LICAR package was used for absolute lipid quantification.
897
898 To ensure the accuracy of the analytical results, we discarded lipids detected in less than 2/3 of
899 the samples, and missing values were estimated using the lower limit from the corresponding

lipid[87].

Screening for differential plasma metabolites and lipids

To identify differential plasma metabolites and lipids, we first calculated VIP scores using PLS-DA in the R package MetaboAnalystR (version 4.0)[88]. We analyzed metabolites with VIP scores $\geqslant$ 1 as differentially abundant metabolites and lipids for downstream data analysis. For details on the metabolites and lipids, see Supplementary Tables 2 and 3.

Fuzzy c-means clustering

Fuzzy c-means clustering was performed using the R package Mfuzz (version 2.62.0)[89]. We selected the screened differentially abundant metabolites and lipids for clustering.

Plasma metabolite pathway analysis

We performed pathway enrichment analysis of the metabolites obtained from fuzzy c-means clustering by group separately using the pathway analysis module in the MetaboAnalystR package. For bubble plots, we selected metabolic pathways with p values $\leqslant$ 0.05 and impacts $\geqslant$ 0.1[90].

Linear mixed model

Since the assumption of independence cannot be met for repeated measurements, zone group data, and spatially correlated data, the above data are often analyzed using linear mixed-effects models (e.g., correlation analysis)[91]. The following model was implemented:

$$Y \sim X + (X \mid \text{Random Effects})$$

Mixed linear models include both fixed and random effects, where fixed effects are the variables under study and random effects are the influences that we wish to control for, which are referred to as “Groups” in this paper. The mixed linear model was generated using the R package statistical function lme4 (version 1.1-35.1). We tested the difference between the fixed-effects model and the model with fixed effects removed through ANOVA to determine whether the linear correlation between the fixed effects was significant.

Quantification and statistical analysis

Statistical analysis was performed using R (version 4.3.1). The Wilcoxon rank-sum test was used in this study. Multiple comparison adjustments were performed using the Benjamini-Hochberg method. $^{*}p < 0.05$, $^{**}p < 0.01$, $^{***}p < 0.001$.

960 **FIGURE LEGENDS**

961 **Figure 1. Overview of the multi-omics profiling of metabolic molecules and immune**
962 **responses in mountain climbers.**

963 (A) Flowchart depicting the overall mountaineering design, sample collection and multi-omics
964 data analysis. All the data were collected from 11 healthy mountain climbers. The figures were
965 created with Adobe Illustrator 2023 and BioRender.com.

966 (B) Effects of high altitude on heart rate (HR) and blood saturation (SpO_2) during mountaineering.
967 Red represents HR, blue represents SpO_2, and the black dotted line represents altitude. M was
968 measured in the morning, and E was measured in the evening.

969 (C) Violin plots showing significant changes in selected routine blood parameters and C-reactive
970 protein (CRP) levels before (D1) and after (D16) the mountaineering expedition. The two-sided *p*
971 values from the paired Wilcoxon rank-sum test are shown, $^{*}p < 0.05$, $^{**}p < 0.01$, $^{***}p < 0.001$.

972 (D) Bar plots showing changes in the numbers of significantly differentially abundant metabolites
973 and complex lipids during mountaineering.

974 (E) Uniform manifold approximation and projection (UMAP) plot showing 15 cell types among
975 375,722 circulating immune cells. Cells are colored according to different cell subtypes.

976 (F) Boxplots showing the relative proportion changes in selected subsets during mountaineering
977 (day 1, day 4, day 7, day 11 and day 16, n = 11); sample points from the same mountain climber
978 are connected with the same color. The two-sided *p* values from the paired Wilcoxon rank-sum
979 test are shown, $^{*}p < 0.05$, $^{**}p < 0.01$, $^{***}p < 0.001$.

980

981 **Figure 2. Dynamic changes in the inflammatory response in monocytes and DCs.**

982 (A) UMAP plot showing nine myeloid cell subsets.

983 (B) Dot plots depicting the percentages and average expression levels of the canonical genes in
984 nine subsets of myeloid cells.

985 (C) Boxplots showing the changes in the relative proportions of selected myeloid cell subsets
986 before and during mountaineering (day 1, day 4, day 7, day 11 and day 16, n = 11); sample points
987 from the same mountain climber are connected with the same color. The two-sided *p* values from
988 the paired Wilcoxon rank-sum test are shown, $^{*}p < 0.05$, $^{**}p < 0.01$, $^{***}p < 0.001$.

989 (D) Heatmap showing the scaled expression of genes in important biological pathways mediated

990 by myeloid cells across different time points. The two-sided *p* values from the Wilcoxon rank-sum
991 test are shown, $^{*}p < 0.05$, $^{**}p < 0.01$, $^{***}p < 0.001$.
992 (E) Violin plots showing dynamic changes in the expression of selected differentially expressed
993 genes (DEGs) in $CCL3^{+}$ $CD14^{+}$ Monos, cDC2s and $CD16^{+}$ Monos ($|\log_2 FC| \geqslant 0.7$, adjusted $p <$
994 0.05). $^{*}p < 0.05$, $^{**}p < 0.01$, $^{***}p < 0.001$.
995 (F) Heatmap showing the regulon areas under the curve per cell (AUCell) scores for myeloid cells
996 across the five time points, calculated using the SCENIC algorithm.
997 (G) Correlation analysis between hypoxia scores and inflammatory response scores for each
998 climber at all five time points (linear mixed model).
999 (H) Dot plots showing the scaled expression and percentages of *HIF1A* in myeloid cell subsets
1000 across different time points. The two-sided *p* values from the Wilcoxon rank-sum test are shown,
1001 $^{*}p < 0.05$, $^{**}p < 0.01$, $^{***}p < 0.001$.
1002
1003 **Figure 3. Dynamic changes in the functional status of T and NK cells in mountain climbers.**
1004 (A) UMAP plot showing nine subsets of $CD8^{+}$ T cells and other cells.
1005 (B) Dot plots depicting the percentages and average expression of the canonical genes in nine
1006 subsets of $CD8^{+}$ T cells and other cells.
1007 (C) Boxplots showing the relative proportions of selected T and NK cell subsets during
1008 mountaineering (day 1, day 4, day 7, day 11 and day 16, n = 11); sample points from the same
1009 mountain climber are connected with the same color. The two-sided *p* values from the paired
1010 Wilcoxon rank-sum test are shown, $^{*}p < 0.05$, $^{**}p < 0.01$, $^{***}p < 0.001$.
1011 (D) Heatmap showing the scaled scores for important immune-related pathways in cytotoxic $CD8^{+}$
1012 T, γδT, $CD16^{+}$ NK and $CD8^{+}$ Tem cells at different time points. The two-sided *p* values from the
1013 Wilcoxon rank-sum test are shown, $^{*}p < 0.05$, $^{**}p < 0.01$, $^{***}p < 0.001$.
1014 (E) Heatmap showing the expression levels of cytotoxicity-related genes in cytotoxic $CD8^{+}$ T, γδT,
1015 $CD16^{+}$ NK and $CD8^{+}$ Tem cells at different time points. The two-sided *p* values from the
1016 Wilcoxon rank-sum test are shown, $^{*}p < 0.05$, $^{**}p < 0.01$, $^{***}p < 0.001$.
1017 (F) Violin plots showing dynamic changes in the expression of selected DEGs in cytotoxic $CD8^{+}$
1018 T, γδT, $CD16^{+}$ NK and $CD8^{+}$ Tem cells ($|\log_2 FC| \geqslant 0.7$, adjusted $p < 0.05$). $^{*}p < 0.05$, $^{**}p < 0.01$,
1019 $^{***}p < 0.001$.

1020 (G) Heatmap showing the regulon AUCell scores for $CD8^+$ T cells across the five time points,
1021 calculated using the SCENIC algorithm.
1022 (H) UMAP plots showing the regulon activities of *EOMES* and *TBX21* on D4 and D16 in $CD8^+$ T
1023 cells, color-coded by AUCell score.
1024
1025 **Figure 4. Activation of the unfolded protein response in plasma B cells during**
1026 **mountaineering.**
1027 (A) UMAP plot showing eight B cell subsets.
1028 (B) Dot plots depicting the percentages and average expression levels of the canonical genes in
1029 eight subsets of B cells.
1030 (C) Boxplots showing the relative proportions of selected B cell subsets during mountaineering
1031 (day 1, day, day 7, day 11 and day 16, n = 11); sample points from the same mountain climber are
1032 connected with the same color. The two-sided p values from the paired Wilcoxon rank-sum test
1033 are shown, $^{*}p < 0.05$, $^{**}p < 0.01$, $^{***}p < 0.001$.
1034 (D) Violin plots showing dynamic changes in the expression of selected DEGs in activated B
1035 cells($|\log_2 FC| \geqslant 0.7$, adjusted $p < 0.05$). $^{*}p < 0.05$, $^{**}p < 0.01$, $^{***}p < 0.001$.
1036 (E) The fifteen enriched biological processes according to Gene Ontology (GO) analysis of the
1037 upregulated DEGs in plasma B cells. Dot color indicates the statistical significance of the
1038 enrichment, and dot size represents the gene ratio annotated to each term.
1039 (F) Heatmap illustrating scaled expression values of selected DEGs across time points in plasma B
1040 cells ($|\log_2 FC| \geqslant 0.7$, adjusted $p < 0.05$). $^{*}p < 0.05$, $^{**}p < 0.01$, $^{***}p < 0.001$.
1041 (G) Heatmap showing the regulon AUCell scores from plasma B cells across different time points,
1042 calculated using the SCENIC algorithm.
1043 (H) Correlation analysis between hypoxia scores and *XBP1* expression levels in plasma B cells for
1044 each climber all five time points (linear mixed model).
1045
1046 **Figure 5. Metabolic profile of circulating immune cells during mountaineering.**
1047 (A) Heatmap showing the scaled scores for oxidative phosphorylation and glycolysis pathways
1048 across different time points in selected cell subsets. The two-sided p values from the Wilcoxon
1049 rank-sum test are shown, $^{*}p < 0.05$, $^{**}p < 0.01$, $^{***}p < 0.001$.

1050 (B) Heatmap showing the average expression of selected genes from oxidative phosphorylation
1051 pathways in myeloid cells across different time points.
1052 (C) Violin plots showing dynamic changes in the expression of *ATP5F1E* in $CCL3^+$ $CD14^+$ Monos,
1053 $FCN1^+$ $CD14^+$ Monos, $C1^+$ $CD16^+$ Monos and cDC2s ($|\log_2 FC| \geqslant 0.7$, adjusted $p < 0.05$). $^*p <$
1054 0.05, $^{**}p < 0.01$, $^{***}p < 0.001$.
1055 (D) Violin plots showing dynamic changes in the expression of *COX4I1*, *COX7A2*, *COX5B* and
1056 *COX7C* in IFN^+ $CD16^+$ Monos ($|\log_2 FC| \geqslant 0.7$, adjusted $p < 0.05$). $^*p < 0.05$, $^{**}p < 0.01$, $^{***}p <$
1057 0.001.
1058 (E) Violin plots showing dynamic changes in the expression of glycolysis-related genes in plasma
1059 B cells and $CD8^+$ Tems ($|\log_2 FC| \geqslant 0.7$, adjusted $p < 0.05$). $^*p < 0.05$, $^{**}p < 0.01$, $^{***}p < 0.001$.
1060 (F) Dynamic changes in AMPK-related pathways ('CAMKK AMPK Signaling Cascade') during
1061 high-altitude mountaineering in different immune cell subsets. Stage 1 is the acclimatization
1062 period, and stage 2 is the extreme altitude mountaineering period. Dots represent the mean $\log_2$-
1063 fold change relative to baseline (D1).
1064 (G) The biological processes that significantly changed during high-altitude mountaineering in
1065 $FCN1^+$ $CD14^+$ Monos, $CD16^+$ Monos, cDC2s and cytotoxic $CD8^+$ T cells included the AMPK
1066 signaling, inflammatory response, hypoxia and immune effector process pathways. Dots represent
1067 the mean $\log_2$-fold change relative to baseline (D1).
1068
1069 **Figure 6. Oxidative stress response of circulating immune cells during mountaineering.**
1070 (A) Heatmap showing the scaled scores for reactive oxygen species, oxidative stress and oxidant
1071 detoxification-related pathways across different time points. The two-sided p values from the
1072 Wilcoxon rank-sum test are shown, $^*p < 0.05$, $^{**}p < 0.01$, $^{***}p < 0.001$.
1073 (B) Correlation analysis between hypoxia scores and oxidative stress scores for each climber at all
1074 five time points (linear mixed model).
1075 (C) Heatmap showing the scaled expression of selected genes from cellular oxidant detoxification
1076 pathways in circulating immune cells across different time points. The two-sided p values from
1077 the Wilcoxon rank-sum test are shown, $^*p < 0.05$, $^{**}p < 0.01$, $^{***}p < 0.001$.
1078 (D) Dot plots showing the scaled average expression levels and percentages of *SOD2* and *NFE2L2*
1079 in selected immune cell subsets at different time points. The two-sided p values from the

1080 Wilcoxon rank-sum test are shown, $^{*}p < 0.05$, $^{**}p < 0.01$, $^{***}p < 0.001$.

1081

1082 **Figure 7. Time series analysis of plasma metabolomics and lipidomic data during high-**
1083 **altitude mountaineering.**

1084 (A) Variable importance in projection (VIP) scores showing the top 15 differentially abundant
1085 metabolites for each sampling point. The heatmap on the right displays the scaled value of the
1086 metabolite at each time point.

1087 (B) Clustering of differentially abundant metabolites and lipids. The circular plots on the right
1088 show the percentage of differentially abundant metabolites and lipids for each cluster.

1089 (C) Pathway enrichment analysis of metabolites from cluster 1 and cluster 4. The red horizontal
1090 dashed line indicates the threshold of statistical significance for the y-axis calculated by the
1091 hypergeometric test ($p < 0.05$). The red vertical dashed lines indicate pathway impact values $\geqslant$
1092 0.1.

1093 (D) The dynamic changes in key metabolites in the enrichment pathways of cluster 1 and cluster 4.
1094 Dots represent the mean $\log_2$-fold change relative to D1, and horizontal bars represent the standard
1095 error of the mean (SEM).

1096 (E) Dynamic changes in oxidative stress-related metabolites during mountaineering. The dots
1097 represent the mean $\log_2$-fold change relative to day 1, and the bars represent the standard error of
1098 the mean (SEM).

1099 (F) Correlation analysis between oxidative stress scores and selenocompound metabolism scores
1100 for each climber at all five time points (linear mixed model).

1101 (G) Stacked column charts showing the percentage of each complex lipid in cluster 2 and cluster 3.

1102 (H) Chemical classification enrichment analysis of complex lipids. The pathway direction is the
1103 change in significant molecules in each classification relative to D1 (blue, downregulated; red,
1104 upregulated). The size of the dot represents the significance of the pathway.

1105

1106 **SUPPLEMENTAL INFORMATION**

1107 **Supplementary Figure 1. Effects of high altitude on physiological parameters during**
1108 **mountaineering.**

1109 (A) Box plots showing the dynamic changes in SpO_2 and heart ratHR with increasing altitude;

1110 sample points from the same mountain climber are connected with the same color (n = 11). The
1111 two-sided *p* values from the paired Wilcoxon rank-sum test are shown, $^{*}p < 0.05$, $^{**}p < 0.01$, $^{***}p <$
1112 0.001.
1113 (B) Box plots showing the changes in SpO_2 and HR when re-exposed to the same altitude (4,400
1114 m and 5,500 m); sample points from the same mountain climber are connected with the same
1115 color (n = 11). The two-sided *p* values from the paired Wilcoxon rank-sum test are shown, $^{*}p <$
1116 0.05, $^{**}p < 0.01$, $^{***}p < 0.001$.
1117 (C) Box plots showing the changes in body composition during mountaineering; sample points
1118 from the same mountain climber are connected with the same color. The two-sided *p* values from
1119 the paired Wilcoxon rank-sum test are shown, but no significant differences were detected. Body
1120 mass index (BMI), body fat percentage (BFP%), muscle mass (MM, kg) and fat mass (FM, kg)
1121 were measured.
1122
1123 **Supplementary Figure 2. Effects of high altitude on routine blood parameters during**
1124 **mountaineering.**
1125 Violin plots showing the changes in routine blood parameters before (D1) and after (D16)
1126 mountaineering, divided into three groups: red blood cell-related parameters, platelet-related
1127 parameters and white blood cell-related parameters. The complete names of these parameters are
1128 displayed in Table S1. The two-sided *p* values from the paired Wilcoxon rank-sum test are shown,
1129 $^{*}p < 0.05$, $^{**}p < 0.01$, $^{***}p < 0.001$.
1130
1131 **Supplementary Figure 3. Quality control of the scRNA-seq data.**
1132 (A) Violin plots showing the distributions of gene counts per cell, unique molecular identifier
1133 (UMI) per cell, and percentage of mitochondrial transcripts per cell across five time points from
1134 eleven mountain climbers.
1135 (B) Bar plots showing the number of cells at each time point and the number of cells from each
1136 volunteer. D1 (n = 69,847 cells), D4 (n = 100,271 cells), D9 (n = 48,686 cells), D11 (n = 97,447
1137 cells), and D16 (n = 5,9471 cells).
1138
1139 **Supplementary Figure 4. Single-cell analysis of circulating immune cells in mountain**

1140 **climbers.**

1141 (A) Violin plots depicting the normalized expression levels of canonical markers associated with
1142 each main immune cell subgroup.

1143 (B) Stacked column charts showing the proportions of each cell type from each volunteer and
1144 different sampling time points.

1145 (C) Boxplots showing the relative proportions of immune cell subsets during mountaineering (day
1146 1, day 4, day 7, day 11 and day 16, n = 11); sample points from the same mountain climber are
1147 connected with the same color. The two-sided *p* values from the paired Wilcoxon rank-sum test
1148 are shown, $^{*}p < 0.05$, $^{**}p < 0.01$, $^{***}p < 0.001$.

1149 (D) UMAP plot of all immune cell subtypes identified from single-cell samples from climbers at
1150 different time points, colored according to their respective subgroup.

1151

1152 **Supplementary Figure 5. Transcriptional changes in monocyte subsets during**
1153 **mountaineering.**

1154 (A) Stacked column charts showing the proportions of myeloid cell subsets from each volunteer
1155 and different sampling time points.

1156 **(B)** Boxplots showing the relative proportions of myeloid cell subsets during mountaineering (day
1157 1, day 4, day 7, day 11 and day 16, n = 11); sample points from the same mountain climber are
1158 connected with the same color. The two-sided *p* values from the paired Wilcoxon rank-sum test
1159 are shown, $^{*}p < 0.05$, $^{**}p < 0.01$, $^{***}p < 0.001$.

1160 (C) Dot plots showing the enriched biological processes by GO analysis of upregulated and
1161 downregulated DEGs on day 4, day 7, day 11 and day 16 compared to day 1. Dot color indicates
1162 the statistical significance of the enrichment, and dot size represents the gene ratio annotated to
1163 each term.

1164 (D) Violin plots showing dynamic changes in the expression of selected DEGs in $FCN1^{+}$ $CD14^{+}$
1165 Monos ($|\log_2 FC| \geqslant 0.7$, adjusted $p < 0.05$). $^{*}p < 0.05$, $^{**}p < 0.01$, $^{***}p < 0.001$.

1166

1167 **Supplementary Figure 6. Transcriptional changes in pDCs during mountaineering.**

1168 (A) The twenty enriched biological processes identified by GO analysis of downregulated DEGs
1169 in pDCs. The dot color indicates the statistical significance of the enrichment, and the dot size

1170 represents the ratio of genes annotated to each term.

1171 (B) Heatmap illustrating scaled expression values of selected DEGs at various time points in pDCs.

1172 The two-sided *p* values from the Wilcoxon rank-sum test are shown, $^{*}p < 0.05$, $^{**}p < 0.01$, $^{***}p <$

1173 0.001.

1174 (C) Heatmap showing the regulon scenic scores for pDCs across different time points, calculated

1175 using the SCENIC algorithm.

1176

1177 **Supplementary Figure 7. Changes in transcription in CD4^{+} T, CD8^{+} T and NK cell subsets**

1178 **during mountaineering.**

1179 (A) UMAP plot showing six subsets of CD4^{+} T cells.

1180 (B) Dot plot depicting the percentages and average expression levels of canonical genes in six

1181 subsets of CD4^{+} T cells.

1182 (C) UMAP plot showing five NK cell subsets.

1183 (D) Dot plot depicting the percentages and average expression levels of canonical genes in five

1184 NK cell subsets.

1185 (E) Box plots showing the changes in the alpha/beta T cell activation pathway over time in naive

1186 CD4^{+} T and Th2 cells; sample points from the same mountain climber are connected with the

1187 same color. The two-sided *p* values from the paired Wilcoxon rank-sum test are shown, $^{*}p < 0.05$,

1188 $^{**}p < 0.01$, $^{***}p < 0.001$.

1189 (F) The regulatory networks of *TBX21* and *EOMES* and their target genes in CD8^{+} T cells.

1190

1191 **Supplementary Figure 8. Dynamic changes in the proportions of CD4^{+} T, CD8+ T and NK**

1192 **cell subsets in mountain climbers.**

1193 (A) Stacked column charts showing the proportions of CD4^{+} T cell subsets from each volunteer

1194 and different sampling time points.

1195 (B) Stacked column charts showing the proportions of CD8^{+} T cell subsets from each volunteer

1196 and at different sampling time points.

1197 (C) Stacked column charts showing the proportions of NK cell subsets from each volunteer and

1198 different sampling time points.

1199 (D) Boxplots illustrating the relative proportions of identified subsets of CD4^{+} T, CD8^{+} T and NK

1200 cells during mountaineering (day 1, day 4, day 7, day 11 and day 16, n = 11); sample points from
1201 the same mountain climber are connected in the same color. The two-sided *p* values from the
1202 paired Wilcoxon rank-sum test are shown, $^{*}p < 0.05$, $^{**}p < 0.01$, $^{***}p < 0.001$.
1203
1204 **Supplementary Figure 9. Dynamic changes in the compositions of B cell subsets in mountain**
1205 **climbers.**
1206 (A) Stacked column charts showing the proportions of B cell subsets from each volunteer and
1207 different sampling time points.
1208 (B) Boxplots showing the relative proportions of B cell subsets during mountaineering (day 1, day
1209 4, day 7, day 11 and day 16, n = 11); sample points from the same mountain climber are
1210 connected with the same color. The two-sided *p* values from the paired Wilcoxon rank-sum test
1211 are shown, $^{*}p < 0.05$, $^{**}p < 0.01$, $^{***}p < 0.001$.
1212 (C) Regulatory networks of *XBP1* and its target genes in plasma B cells.
1213
1214 **Supplementary Figure 10. Metabolic pathway analysis of circulating immune cells in**
1215 **mountain climbers.**
1216 (A) Heatmap showing the scaled expression of genes in the hypoxia pathway and dot plots
1217 illustrating the scaled expression and percentages of *HIF1A* in the T, NK and B cell subgroups
1218 across different time points. The two-sided *p* values from the Wilcoxon rank-sum test are shown,
1219 $^{*}p < 0.05$, $^{**}p < 0.01$, $^{***}p < 0.001$.
1220 (B) Heatmap showing the scaled expression of genes in AMPK-related pathways ('CAMKK
1221 AMPK Signaling Cascade') across different time points. The two-sided *p* values from the
1222 Wilcoxon rank-sum test are shown, $^{*}p < 0.05$, $^{**}p < 0.01$, $^{***}p < 0.001$.
1223 (C) Heatmap showing the expression levels of AMPK-related genes in immune cell subgroups
1224 across different time points. The two-sided *p* values from the Wilcoxon rank-sum test are shown,
1225 $^{*}p < 0.05$, $^{**}p < 0.01$, $^{***}p < 0.001$.
1226
1227 **Supplementary Figure 11. Hypoxia-induced glycolysis pathway during mountaineering.**
1228 Correlation analysis between hypoxia scores and glycolysis scores in immune cells (A) and each
1229 immune subgroup (B) (linear mixed model).

1230

1231 **Supplementary Figure 12. Alterations in plasma metabolites during mountaineering.**

1232 (A) Sankey diagram illustrating the metabolites contained in metabolic pathways that were
1233 enriched in cluster 1 and cluster 4.

1234 (B) Pathway enrichment analysis of metabolites from cluster 2 and cluster 3. The red horizontal
1235 dashed line indicates the threshold of statistical significance for the y-axis calculated by the
1236 hypergeometric test ($p < 0.05$). The red vertical dashed lines indicate pathway impact values $\geqslant$
1237 0.1.

1238 (C) Dynamic changes in key metabolites in the citrate cycle (TCA cycle). Dots represent the mean
1239 $\log_2$-fold change relative to D1, and horizontal bars represent the standard error of the mean
1240 (SEM).

1241 (D) Heatmaps representing changes in the levels of carnitines or acylcarnitines and fatty acids.
1242 Clusters are labeled on the left side of the heatmap. Fatty acids with different chain lengths are
1243 indicated by different colors.

1244 (E) Box plots representing the 3-hydroxybutyric acid levels at different time points; the horizontal
1245 line represents the median value. The p values from the two-sided Wilcoxon rank-sum test are
1246 shown, $^{*}p < 0.05$, $^{**}p < 0.01$, $^{***}p < 0.001$.

1247

1248

1249

1250

1251

1252

1253

1254

1255

1256

1257

1258

1259

REFERENCES

1. Apollo, M., *The true accessibility of mountaineering: The case of the High Himalaya.* Journal of Outdoor Recreation and Tourism, 2017. **17**: p. 29-43.
2. Luks, A.M. and P.H. Hackett, *Medical Conditions and High-Altitude Travel Reply.* New England Journal of Medicine, 2022. **386**(19): p. 1866-1867.
3. Palmer, B.F., *Physiology and Pathophysiology With Ascent to Altitude.* American Journal of the Medical Sciences, 2010. **340**(1): p. 69-77.
4. Burtscher, J., et al., *Immune consequences of exercise in hypoxia: A narrative review.* J Sport Health Sci, 2023.
5. Bosco, G., et al., *Body Composition and Endocrine Adaptations to High-Altitude Trekking in the Himalayas.* Advancements and Innovations in Health Sciences, 2019. **1211**: p. 61-68.
6. Basnyat, B. and J.M. Starling, *Infectious Diseases at High Altitude.* Microbiol Spectr, 2015. **3**(4).
7. Simpson, R.J., et al., *Can exercise affect immune function to increase susceptibility to infection?* Exercise Immunology Review, 2020. **26**: p. 8-22.
8. Nieman, D.C. and L.M. Wentz, *The compelling link between physical activity and the body's defense system.* Journal of Sport and Health Science, 2019. **8**(3): p. 201-217.
9. Manella, G., et al., *The human blood transcriptome exhibits time-of-day-dependent response to hypoxia: Lessons from the highest city in the world.* Cell Reports, 2022. **40**(7).
10. Rohm, I., et al., *Hypobaric hypoxia in 3000 m altitude leads to a significant decrease in circulating plasmacytoid dendritic cells in humans.* Clin Hemorheol Microcirc, 2016. **63**(3): p. 257-65.
11. Facco, M., et al., *Modulation of immune response by the acute and chronic exposure to high altitude.* Medicine and Science in Sports and Exercise, 2005. **37**(5): p. 768-774.
12. Chen, F., et al., *Transcriptome and Network Changes in Climbers at Extreme Altitudes.* Plos One, 2012. **7**(2).
13. Miller, L.E., et al., *Blood Oxidative-Stress Markers During a High-Altitude Trek.* International Journal of Sport Nutrition and Exercise Metabolism, 2013. **23**(1): p. 65-72.
14. Mrakic-Sposta, S., et al., *OxInflammation at High Altitudes: A Proof of Concept from the Himalayas.* Antioxidants, 2022. **11**(2).

1290 15. Nieman, D.C. and B.D. Pence, *Exercise immunology: Future directions.* Journal of Sport and
1291 Health Science, 2020. **9**(5): p. 432-445.
1292 16. Mariggiò, M.A., et al., *Peripheral Blood Lymphocytes: A Model for Monitoring*
1293 *Physiological Adaptation to High Altitude.* High Altitude Medicine & Biology, 2010. **11**(4): p.
1294 333-342.
1295 17. Morabito, C., et al., *Responses of peripheral blood mononuclear cells to moderate exercise*
1296 *and hypoxia.* Scandinavian Journal of Medicine & Science in Sports, 2016. **26**(10): p. 1188-
1297 1199.
1298 18. Chi, H.B., *Immunometabolism at the intersection of metabolic signaling, cell fate, and*
1299 *systems immunology.* Cellular & Molecular Immunology, 2022. **19**(3): p. 299-302.
1300 19. O'Brien, K.A., et al., *Metabolomic and lipidomic plasma profile changes in human*
1301 *participants ascending to Everest Base Camp.* Scientific Reports, 2019. **9**.
1302 20. Yu, Y.L., et al., *Single-cell sequencing of immune cells after marathon and symptom-limited*
1303 *cardiopulmonary exercise.* Iscience, 2023. **26**(4).
1304 21. Ehrchen, J.M., et al., *The endogenous Toll-like receptor 4 agonist S100A8/S100A9*
1305 *(calprotectin) as innate amplifier of infection, autoimmunity, and cancer.* Journal of
1306 Leukocyte Biology, 2009. **86**(3): p. 557-566.
1307 22. Swanson, K.V., M. Deng, and J.P.Y. Ting, *The NLRP3 inflammasome: molecular activation*
1308 *and regulation to therapeutics.* Nature Reviews Immunology, 2019. **19**(8): p. 477-489.
1309 23. van de Sande, B., et al., *A scalable SCENIC workflow for single-cell gene regulatory network*
1310 *analysis.* Nature Protocols, 2020. **15**(7): p. 2247-2276.
1311 24. Pham, K., K. Parikh, and E.C. Heinrich, *Hypoxia and Inflammation: Insights From High-*
1312 *Altitude Physiology.* Frontiers in Physiology, 2021. **12**.
1313 25. Lin, N. and M.C. Simon, *Hypoxia-inducible factors: key regulators of myeloid cells during*
1314 *inflammation.* Journal of Clinical Investigation, 2016. **126**(10): p. 3661-3671.
1315 26. Swiecki, M. and M. Colonna, *The multifaceted biology of plasmacytoid dendritic cells.*
1316 Nature Reviews Immunology, 2015. **15**(8): p. 471-485.
1317 27. Iwakoshi, N.N., M. Pypaert, and L.H. Glimcher, *The transcription factor XBP-1 is essential*
1318 *for the development and survival of dendritic cells.* Journal of Experimental Medicine, 2007.
1319 **204**(10): p. 2267-2275.

1320 28. Yilmaz, A., et al., *Decrease in circulating plasmacytoid dendritic cells during short-term*
1321 *systemic normobaric hypoxia.* European Journal of Clinical Investigation, 2016. **46**(2): p.
1322 115-122.
1323 29. Wobben, R., et al., *Role of hypoxia inducible factor-1α for interferon synthesis in mouse*
1324 *dendritic cells.* Biological Chemistry, 2013. **394**(4): p. 495-505.
1325 30. Vignali, D.A.A., L.W. Collison, and C.J. Workman, *How regulatory T cells work.* Nature
1326 Reviews Immunology, 2008. **8**(7): p. 523-532.
1327 31. Fang, M., et al., *CD94 Is Essential for NK Cell-Mediated Resistance to a Lethal Viral*
1328 *Disease.* Immunity, 2011. **34**(4): p. 579-589.
1329 32. Li, Q., et al., *Upregulation of CX3CR1 expression in circulating T cells of systemic lupus*
1330 *erythematosus patients as a reflection of autoimmune status through characterization of*
1331 *cytotoxic capacity.* International Immunopharmacology, 2024. **126**.
1332 33. Le Bouteiller, P., et al., *CD160: A unique activating NK cell receptor.* Immunology Letters,
1333 2011. **138**(2): p. 93-96.
1334 34. Tu, T.C., et al., *CD160 is essential for NK-mediated IFN-γ production.* Journal of
1335 Experimental Medicine, 2015. **212**(3): p. 415-429.
1336 35. Li, M.O. and R.A. Flavell, *TGF-β:: A master of all T cell trades.* Cell, 2008. **134**(3): p. 392-
1337 404.
1338 36. Knox, J.J., et al., *Characterization of T-bet and eomes in Peripheral Human immune Cells*
1339 *(vol 5, 217, 2014).* Frontiers in Immunology, 2016. **7**.
1340 37. Krzyzak, L., et al., *CD83 Modulates B Cell Activation and Germinal Center Responses.*
1341 Journal of Immunology, 2016. **196**(9): p. 3581-3594.
1342 38. Ricci, D., T. Gidalevitz, and Y. Argon, *The special unfolded protein response in plasma*
1343 *cells*.* Immunological Reviews, 2021. **303**(1): p. 35-51.
1344 39. Chohan, I.S., et al., *Immune response in human subjects at high altitude.* Int J Biometeorol,
1345 1975. **19**(3): p. 137-43.
1346 40. Reimold, A.M., et al., *Plasma cell differentiation requires the transcription factor XBP-1.*
1347 Nature, 2001. **412**(6844): p. 300-307.
1348 41. Romero-Ramirez, L., et al., *XBP1 is essential for survival under hypoxic conditions and is*
1349 *required for tumor growth.* Cancer Research, 2004. **64**(17): p. 5943-5947.

1350 42. Lee, P., N.S. Chandel, and M.C. Simon, *Cellular adaptation to hypoxia through hypoxia*
1351 *inducible factors and beyond.* Nature Reviews Molecular Cell Biology, 2020. **21**(5): p. 268-
1352 283.
1353 43. Tanner, L.B., et al., *Four Key Steps Control Glycolytic Flux in Mammalian Cells.* Cell
1354 Systems, 2018. **7**(1): p. 49-+.
1355 44. Krzeslak, A., et al., *Expression of GLUT1 and GLUT3 Glucose Transporters in Endometrial*
1356 *and Breast Cancers.* Pathology & Oncology Research, 2012. **18**(3): p. 721-728.
1357 45. Herzig, S. and R.J. Shaw, *AMPK: guardian of metabolism and mitochondrial homeostasis.*
1358 Nature Reviews Molecular Cell Biology, 2018. **19**(2): p. 121-135.
1359 46. Rolf, J., et al., *AMPKα1: A glucose sensor that controls CD8 T-cell memory.* European
1360 Journal of Immunology, 2013. **43**(4): p. 889-896.
1361 47. Wang, J., et al., *The regulation effect of AMPK in immune related diseases.* Science China-
1362 Life Sciences, 2018. **61**(5): p. 523-533.
1363 48. Cui, Y.X., et al., *The role of AMPK in macrophage metabolism, function and polarisation.*
1364 Journal of Translational Medicine, 2023. **21**(1).
1365 49. Blagih, J., et al., *The Energy Sensor AMPK Regulates T Cell Metabolic Adaptation and*
1366 *Effector Responses In Vivo.* Immunity, 2015. **42**(1): p. 41-54.
1367 50. Halliwell, B., *Understanding mechanisms of antioxidant action in health and disease.* Nature
1368 Reviews Molecular Cell Biology, 2024. **25**(1): p. 13-33.
1369 51. Flynn, J.M. and S. Melov, *SOD2 in mitochondrial dysfunction and neurodegeneration.* Free
1370 Radical Biology and Medicine, 2013. **62**: p. 4-12.
1371 52. Kaspar, J.W., S.K. Niture, and A.K. Jaiswal, *Nrf2:INrf2 (Keap1) signaling in oxidative stress.*
1372 Free Radical Biology and Medicine, 2009. **47**(9): p. 1304-1309.
1373 53. Lee, S., S.M. Kim, and R.T. Lee, *Thioredoxin and Thioredoxin Target Proteins: From*
1374 *Molecular Mechanisms to Functional Significance.* Antioxidants & Redox Signaling, 2013.
1375 **18**(10): p. 1165-1207.
1376 54. Zito, E., *PRDX4, an Endoplasmic Reticulum-Localized Peroxiredoxin at the Crossroads*
1377 *Between Enzymatic Oxidative Protein Folding and Nonenzymatic Protein Oxidation.*
1378 Antioxidants & Redox Signaling, 2013. **18**(13): p. 1666-1674.
1379 55. Adeva-Andany, M.M., et al., *Metabolic effects of glucagon in humans.* J Clin Transl

1380 Endocrinol, 2019. **15**: p. 45-53.
1381 56. Tipton, K.D., D.L. Hamilton, and I.J. Gallagher, *Assessing the Role of Muscle Protein*
1382 *Breakdown in Response to Nutrition and Exercise in Humans.* Sports Medicine, 2018. **48**: p.
1383 S53-S64.
1384 57. Lushchak, V.I., *Glutathione homeostasis and functions: potential targets for medical*
1385 *interventions.* J Amino Acids, 2012. **2012**: p. 736837.
1386 58. Yang, L., S. Venneti, and D. Nagrath, *Glutaminolysis: A Hallmark of Cancer Metabolism.*
1387 Annu Rev Biomed Eng, 2017. **19**: p. 163-194.
1388 59. Liu, D., et al., *Moderate altitude exposure impacts host fasting blood glucose and serum*
1389 *metabolome by regulation of the intestinal flora.* Science of the Total Environment, 2023.
1390 **905**.
1391 60. Cruzat, V., et al., *Glutamine: Metabolism and Immune Function, Supplementation and*
1392 *Clinical Translation.* Nutrients, 2018. **10**(11).
1393 61. Jin, Z., S.K. Mendu, and B. Birnir, *GABA is an effective immunomodulatory molecule.*
1394 Amino Acids, 2013. **45**(1): p. 87-94.
1395 62. Schrauzer, G.N., *The nutritional significance, metabolism and toxicology of selenomethionine.*
1396 Adv Food Nutr Res, 2003. **47**: p. 73-112.
1397 63. Ayala, A., M.F. Munoz, and S. Arguelles, *Lipid peroxidation: production, metabolism, and*
1398 *signaling mechanisms of malondialdehyde and 4-hydroxy-2-nonenal.* Oxid Med Cell Longev,
1399 2014. **2014**: p. 360438.
1400 64. Makrecka-Kuka, M., et al., *Plasma acylcarnitine concentrations reflect the acylcarnitine*
1401 *profile in cardiac tissues.* Sci Rep, 2017. **7**(1): p. 17528.
1402 65. Nelson, A.B., et al., *Metabolic Messengers: ketone bodies.* Nat Metab, 2023. **5**(12): p. 2062-
1403 2074.
1404 66. Tsekouras, Y.E., et al., *A single bout of whole-body resistance exercise augments basal*
1405 *VLDL-triacylglycerol removal from plasma in healthy untrained men.* Clin Sci (Lond), 2009.
1406 **116**(2): p. 147-56.
1407 67. Liu, P., et al., *The mechanisms of lysophosphatidylcholine in the development of diseases.*
1408 Life Sci, 2020. **247**: p. 117443.
1409 68. van der Veen, J.N., et al., *The critical role of phosphatidylcholine and*

1410 *phosphatidylethanolamine metabolism in health and disease.* Biochimica Et Biophysica
1411 Acta-Biomembranes, 2017. **1859**(9): p. 1558-1572.
1412 69. Nieman, D.C., et al., *Serum Metabolic Signatures Induced By a Three-Day Intensified*
1413 *Exercise Period Persist After 14 h of Recovery in Runners.* Journal of Proteome Research,
1414 2013. **12**(10): p. 4577-4584.
1415 70. Iqbal, J., et al., *Sphingolipids and Lipoproteins in Health and Metabolic Disorders.* Trends in
1416 Endocrinology and Metabolism, 2017. **28**(7): p. 506-518.
1417 71. Da Rosa, P.C., et al., *The physical exercise-induced oxidative*
1418 *inflammatory response in peripheral blood mononuclear cells: Signaling cellular energetic stress*
1419 *situations.* Life Sciences, 2023. **321**.
1420 72. Laddu, R., et al., *Physical activity for immunity protection: Inoculating populations with*
1421 *healthy living medicine in preparation for the next pandemic.* Progress in Cardiovascular
1422 Diseases, 2021. **64**: p. 102-104.
1423 73. Pham, K., et al., *Inflammatory gene expression during acute high-altitude exposure.* Journal
1424 of Physiology-London, 2022. **600**(18): p. 4169-4186.
1425 74. Spaulding, H.R. and Z. Yan, *AMPK and the Adaptation to Exercise.* Annual Review of
1426 Physiology, 2022. **84**: p. 209-227.
1427 75. Kammerer, T., et al., *Hypoxic-Inflammatory Responses under Acute Hypoxia: In Vitro*
1428 *Experiments and Prospective Observational Expedition Trial.* International Journal of
1429 Molecular Sciences, 2020. **21**(3).
1430 76. McNicholas, W.T., *Chronic Obstructive Pulmonary Disease and Obstructive Sleep Apnea*
1431 *Overlaps in Pathophysiology, Systemic Inflammation, and Cardiovascular Disease.*
1432 American Journal of Respiratory and Critical Care Medicine, 2009. **180**(8): p. 692-700.
1433 77. Rius, J., et al., *NF-κB links innate immunity to the hypoxic response through transcriptional*
1434 *regulation of HIF-1α.* Nature, 2008. **453**(7196): p. 807-U9.
1435 78. Mingyuan, X., et al., *Hypoxia-inducible factor-1alpha activates transforming growth factor-*
1436 *beta1/Smad signaling and increases collagen deposition in dermal fibroblasts.* Oncotarget,
1437 2018. **9**(3): p. 3188-3197.
1438 79. Regis, S., et al., *NK Cell Function Regulation by TGF-β-Induced Epigenetic Mechanisms.*
1439 Frontiers in Immunology, 2020. **11**.

1440 80. Murray, A.J. and J.A. Horscroft, *Mitochondrial function at extreme high altitude.* Journal of
1441 Physiology-London, 2016. **594**(5): p. 1137-1149.
1442 81. Sinha, S., et al., *Different adaptation patterns of antioxidant system in natives and sojourners*
1443 *at high altitude.* Respiratory Physiology & Neurobiology, 2009. **167**(3): p. 255-260.
1444 82. Dobin, A., et al., *STAR: ultrafast universal RNA-seq aligner.* Bioinformatics, 2013. **29**(1): p.
1445 15-21.
1446 83. Butler, A., et al., *Integrating single-cell transcriptomic data across different conditions,*
1447 *technologies, and species.* Nature Biotechnology, 2018. **36**(5): p. 411-+.
1448 84. McGinnis, C.S., L.M. Murrow, and Z.J. Gartner, *DoubletFinder: Doublet Detection in*
1449 *Single-Cell RNA Sequencing Data Using Artificial Nearest Neighbors.* Cell Systems, 2019.
1450 **8**(4): p. 329-+.
1451 85. Yu, G.C., et al., *clusterProfiler: an R Package for Comparing Biological Themes Among*
1452 *Gene Clusters.* Omics-a Journal of Integrative Biology, 2012. **16**(5): p. 284-287.
1453 86. Liberzon, A., *The Molecular Signatures Database (MSigDB) hallmark gene set collection. .*
1454 Cell systems, 2015.
1455 87. Tyanova, S., et al., *The Perseus computational platform for comprehensive analysis of*
1456 *(prote)omics data.* Nature Methods, 2016. **13**(9): p. 731-740.
1457 88. Pang, Z.Q., et al., *Using MetaboAnalyst 5.0 for LC-HRMS spectra processing, multi-omics*
1458 *integration and covariate adjustment of global metabolomics data.* Nature Protocols, 2022.
1459 **17**(8): p. 1735-1761.
1460 89. *Mfuzz: a software package for soft clustering of microarray data.* 2007.
1461 90. Lee, J.W., et al., *Integrated analysis of plasma and single immune cells uncovers metabolic*
1462 *changes in individuals with COVID-19.* Nature Biotechnology, 2022. **40**(1): p. 110-+.
1463 91. Bolker, B.M., et al., *Generalized linear mixed models: a practical guide for ecology and*
1464 *evolution.* Trends in Ecology & Evolution, 2009. **24**(3): p. 127-135.
1465

Figure 1

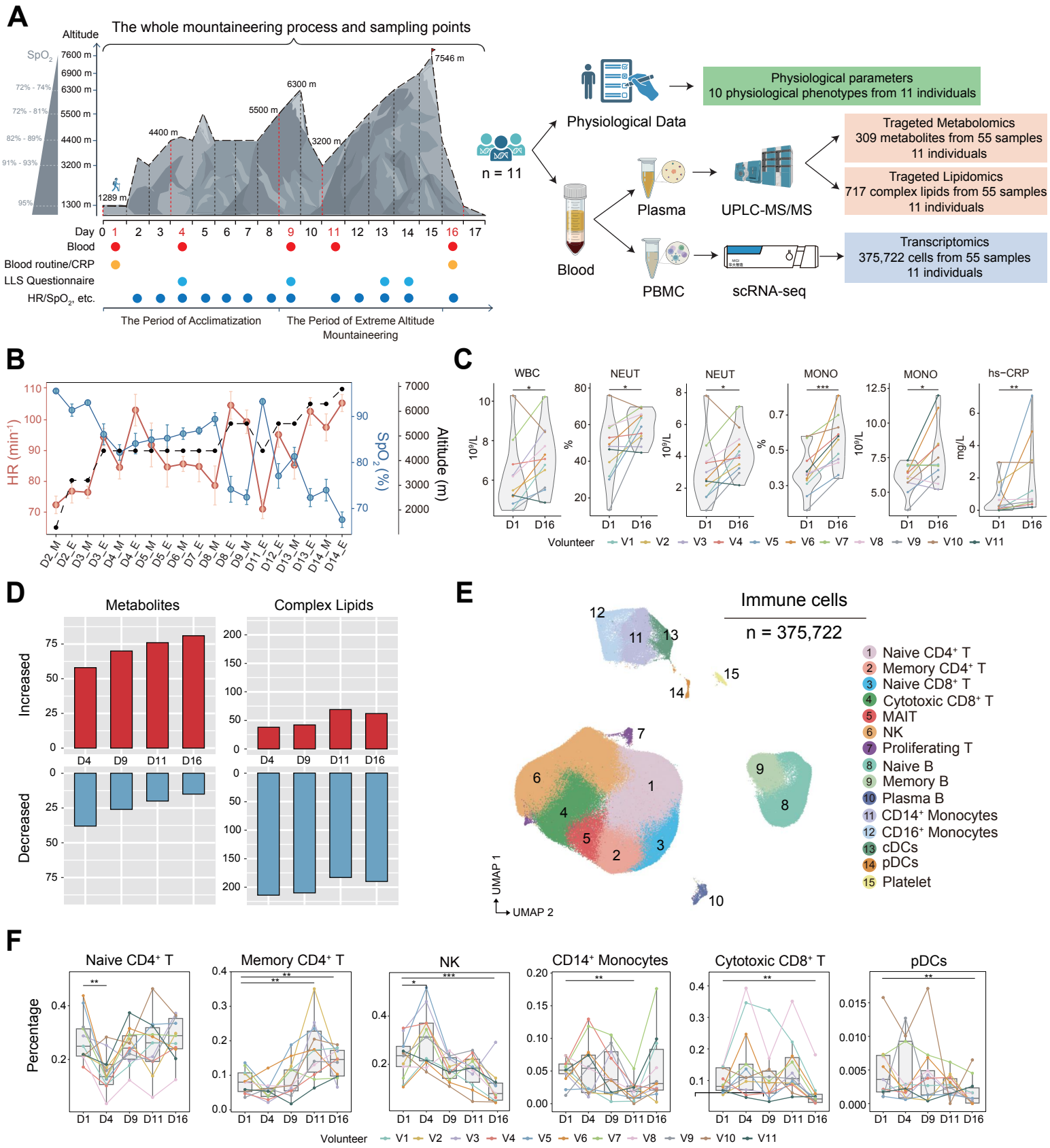
A
The whole mountaineering process and sampling points
Altitude
SpO2
7600 m
6900 m
6300 m
5500 m
4400 m
3200 m
1300 m
1289 m
4400 m
5500 m
6300 m
3200 m
7546 m
Day 0 1 2 3 4 5 6 7 8 9 10 11 12 13 14 15 16 17
Blood
Blood routine/CRP
LLS Questionnaire
HR/SpO2, etc.
The Period of Acclimatization
The Period of Extreme Altitude Mountaineering
n = 11
Physiological Data
Physiological parameters
10 physiological phenotypes from 11 individuals
Blood
Plasma
UPLC-MS/MS
Trageted Metabolomics
309 metabolites from 55 samples
11 individuals
Trageted Lipidomics
717 complex lipids from 55 samples
11 individuals
PBMC
scRNA-seq
Transcriptomics
375,722 cells from 55 samples
11 individuals
B
HR (min-1)
SpO2 (%)
Altitude (m)
C
WBC
NEUT
NEUT
MONO
MONO
hs-CRP
D1 D16
Volunteer V1 V2 V3 V4 V5 V6 V7 V8 V9 V10 V11
D
Metabolites
Complex Lipids
Increased
Decreased
D4 D9 D11 D16
E
Immune cells
n = 375,722
1 Naive CD4+ T
2 Memory CD4+ T
3 Naive CD8+ T
4 Cytotoxic CD8+ T
5 MAIT
6 NK
7 Proliferating T
8 Naive B
9 Memory B
10 Plasma B
11 CD14+ Monocytes
12 CD16+ Monocytes
13 cDCs
14 pDCs
15 Platelet
UMAP 1
UMAP 2
F
Naive CD4+ T
Memory CD4+ T
NK
CD14+ Monocytes
Cytotoxic CD8+ T
pDCs
Percentage
D1 D4 D9 D11 D16
Volunteer V1 V2 V3 V4 V5 V6 V7 V8 V9 V10 V11

Figure 2

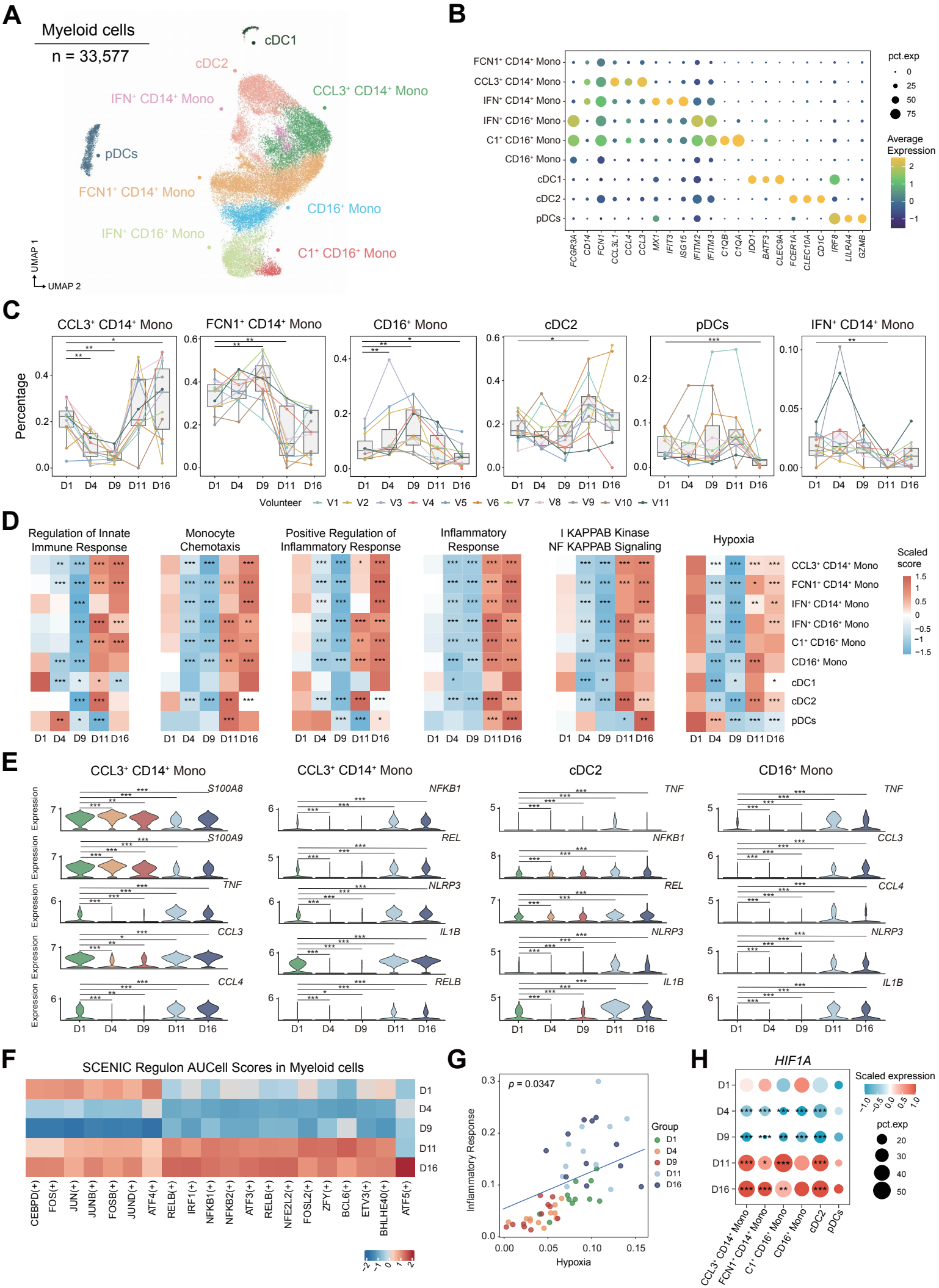
A
Myeloid cells
n = 33,577
cDC1
cDC2
IFN⁺ CD14⁺ Mono
CCL3⁺ CD14⁺ Mono
pDCs
FCN1⁺ CD14⁺ Mono
CD16⁺ Mono
IFN⁺ CD16⁺ Mono
C1⁺ CD16⁺ Mono
UMAP 1
UMAP 2
B
pct.exp
Average Expression
FCGR3A
CD14
FCN1
CCL3L1
CCL4
CCL3
MX1
IFIT3
ISG15
IFITM2
IFITM3
C1QB
C1QA
IDO1
BATF3
CLEC9A
FCER1A
CLEC10A
CD1C
IRF8
LILRA4
GZMB
C
CCL3⁺ CD14⁺ Mono
FCN1⁺ CD14⁺ Mono
CD16⁺ Mono
cDC2
pDCs
IFN⁺ CD14⁺ Mono
Percentage
D1 D4 D9 D11 D16
Volunteer V1 V2 V3 V4 V5 V6 V7 V8 V9 V10 V11
D
Regulation of Innate Immune Response
Monocyte Chemotaxis
Positive Regulation of Inflammatory Response
Inflammatory Response
I KAPPAB Kinase NF KAPPAB Signaling
Hypoxia
Scaled score
E
CCL3⁺ CD14⁺ Mono
cDC2
CD16⁺ Mono
Expression
S100A8
S100A9
TNF
CCL3
CCL4
NFKB1
REL
NLRP3
IL1B
RELB
F
SCENIC Regulon AUCell Scores in Myeloid cells
CEBPD(+)
FOS(+)
JUN(+)
JUNB(+)
FOSB(+)
JUND(+)
ATF4(+)
RELB(+)
IRF1(+)
NFKB1(+)
NFKB2(+)
ATF3(+)
RELB(+)
NFE2L2(+)
FOSL2(+)
ZFY(+)
BCL6(+)
ETV3(+)
BHLHE40(+)
ATF5(+)
G
p = 0.0347
Inflammatory Response
Hypoxia
Group
H
HIF1A
Scaled expression
pct.exp

Figure 3

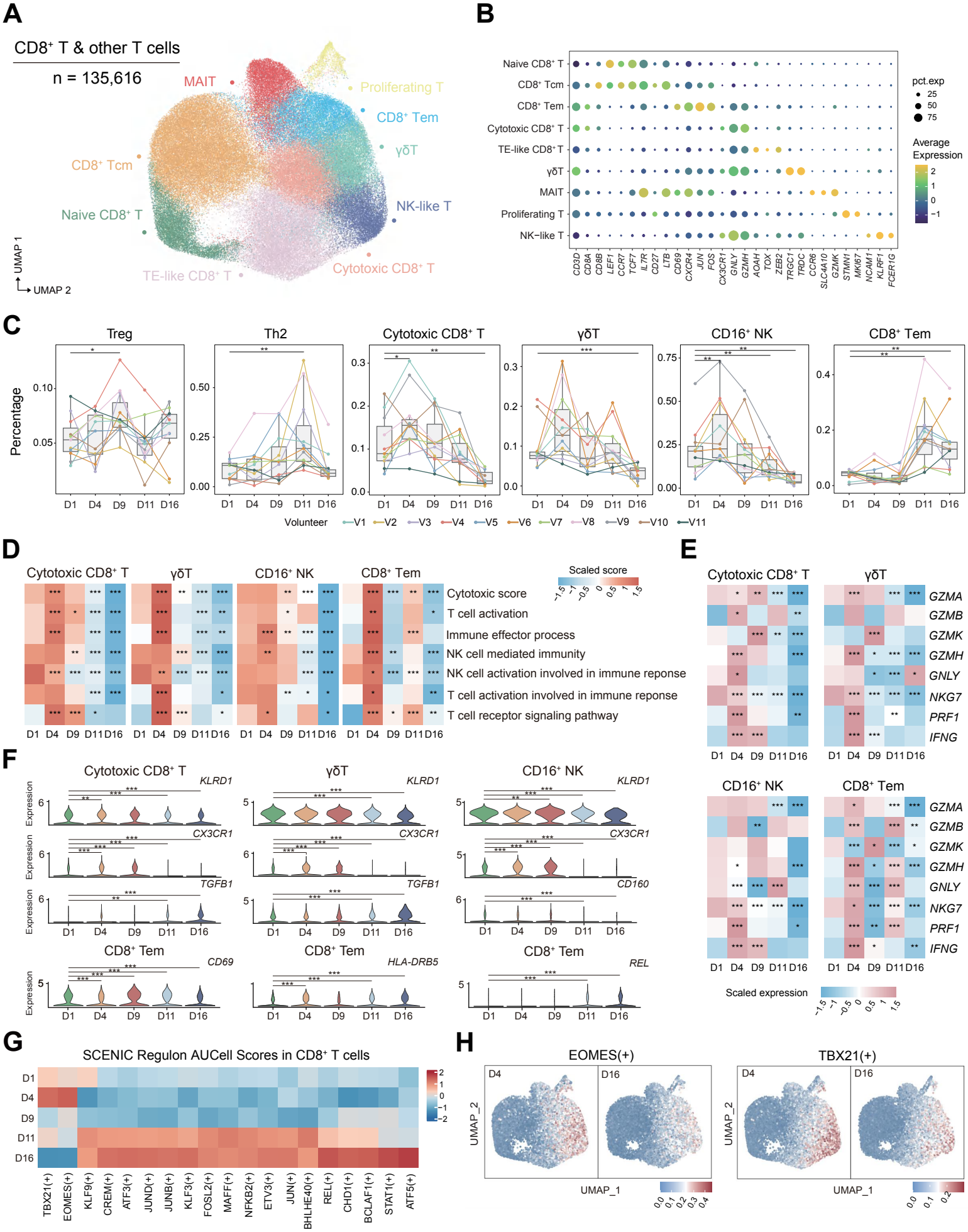
A
CD8⁺ T & other T cells
n = 135,616
MAIT
Proliferating T
CD8⁺ Tem
γδT
CD8⁺ Tcm
NK-like T
Naive CD8⁺ T
TE-like CD8⁺ T
Cytotoxic CD8⁺ T
UMAP 1
UMAP 2
B
Naive CD8⁺ T
CD8⁺ Tcm
CD8⁺ Tem
Cytotoxic CD8⁺ T
TE-like CD8⁺ T
γδT
MAIT
Proliferating T
NK−like T
CD3D CD8A CD8B LEF1 CCR7 TCF7 IL7R CD27 LTB CD69 CXCR4 JUN FOS CX3CR1 GNLY GZMH AOAH TOX ZEB2 TRGC1 TRDC CCR6 SLC4A10 GZMK STMN1 MKI67 NCAM1 KLRF1 FCER1G
pct.exp
25
50
75
Average Expression
C
Treg
Th2
Cytotoxic CD8⁺ T
γδT
CD16⁺ NK
CD8⁺ Tem
Percentage
D1 D4 D9 D11 D16
Volunteer
V1 V2 V3 V4 V5 V6 V7 V8 V9 V10 V11
D
Cytotoxic CD8⁺ T
γδT
CD16⁺ NK
CD8⁺ Tem
Scaled score
Cytotoxic score
T cell activation
Immune effector process
NK cell mediated immunity
NK cell activation involved in immune reponse
T cell activation involved in immune reponse
T cell receptor signaling pathway
E
Cytotoxic CD8⁺ T
γδT
CD16⁺ NK
CD8⁺ Tem
GZMA
GZMB
GZMK
GZMH
GNLY
NKG7
PRF1
IFNG
Scaled expression
F
Cytotoxic CD8⁺ T
γδT
CD16⁺ NK
CD8⁺ Tem
KLRD1
CX3CR1
TGFB1
CD160
CD69
HLA-DRB5
REL
Expression
G
SCENIC Regulon AUCell Scores in CD8⁺ T cells
D1
D4
D9
D11
D16
TBX21(+) EOMES(+) KLF9(+) CREM(+) ATF3(+) JUND(+) JUNB(+) KLF3(+) FOSL2(+) MAFF(+) NFKB2(+) ETV3(+) JUN(+) BHLHE40(+) REL(+) CHD1(+) BCLAF1(+) STAT1(+) ATF5(+)
H
EOMES(+)
TBX21(+)
D4
D16
UMAP_2
UMAP_1

Figure 4

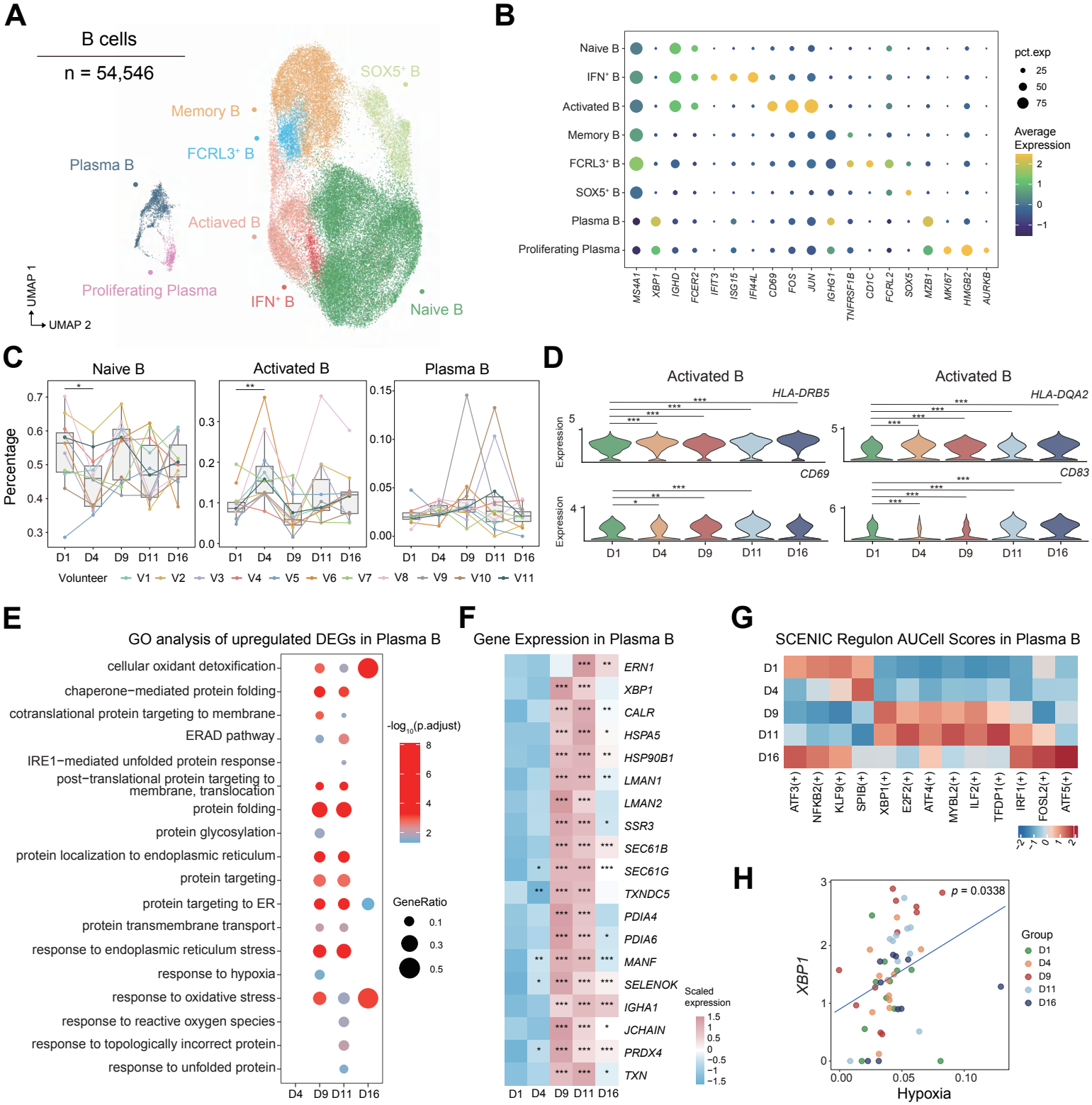
A
B cells
n = 54,546
SOX5⁺ B
Memory B
FCRL3⁺ B
Plasma B
Actiaved B
Proliferating Plasma
IFN⁺ B
Naive B
UMAP 1
UMAP 2
B
Naive B
IFN⁺ B
Activated B
Memory B
FCRL3⁺ B
SOX5⁺ B
Plasma B
Proliferating Plasma
MS4A1 XBP1 IGHD FCER2 IFIT3 ISG15 IFI44L CD69 FOS JUN IGHG1 TNFRSF1B CD1C FCRL2 SOX5 MZB1 MKI67 HMGB2 AURKB
pct.exp
25
50
75
Average Expression
2
1
0
−1
C
Naive B
Activated B
Plasma B
Percentage
D1 D4 D9 D11 D16
Volunteer V1 V2 V3 V4 V5 V6 V7 V8 V9 V10 V11
D
Activated B
HLA-DRB5
HLA-DQA2
CD69
CD83
Expression
D1 D4 D9 D11 D16
E
GO analysis of upregulated DEGs in Plasma B
cellular oxidant detoxification
chaperone−mediated protein folding
cotranslational protein targeting to membrane
ERAD pathway
IRE1−mediated unfolded protein response
post−translational protein targeting to membrane, translocation
protein folding
protein glycosylation
protein localization to endoplasmic reticulum
protein targeting
protein targeting to ER
protein transmembrane transport
response to endoplasmic reticulum stress
response to hypoxia
response to oxidative stress
response to reactive oxygen species
response to topologically incorrect protein
response to unfolded protein
D4 D9 D11 D16
-log10(p.adjust)
8
6
4
2
GeneRatio
0.1
0.3
0.5
F
Gene Expression in Plasma B
ERN1
XBP1
CALR
HSPA5
HSP90B1
LMAN1
LMAN2
SSR3
SEC61B
SEC61G
TXNDC5
PDIA4
PDIA6
MANF
SELENOK
IGHA1
JCHAIN
PRDX4
TXN
D1 D4 D9 D11 D16
Scaled expression
1.5
1
0.5
0
−0.5
−1
−1.5
G
SCENIC Regulon AUCell Scores in Plasma B
D1
D4
D9
D11
D16
ATF3(+) NFKB2(+) KLF9(+) SPIB(+) XBP1(+) E2F2(+) ATF4(+) MYBL2(+) ILF2(+) TFDP1(+) IRF1(+) FOSL2(+) ATF5(+)
H
p = 0.0338
XBP1
Hypoxia
Group
D1
D4
D9
D11
D16

Figure 5

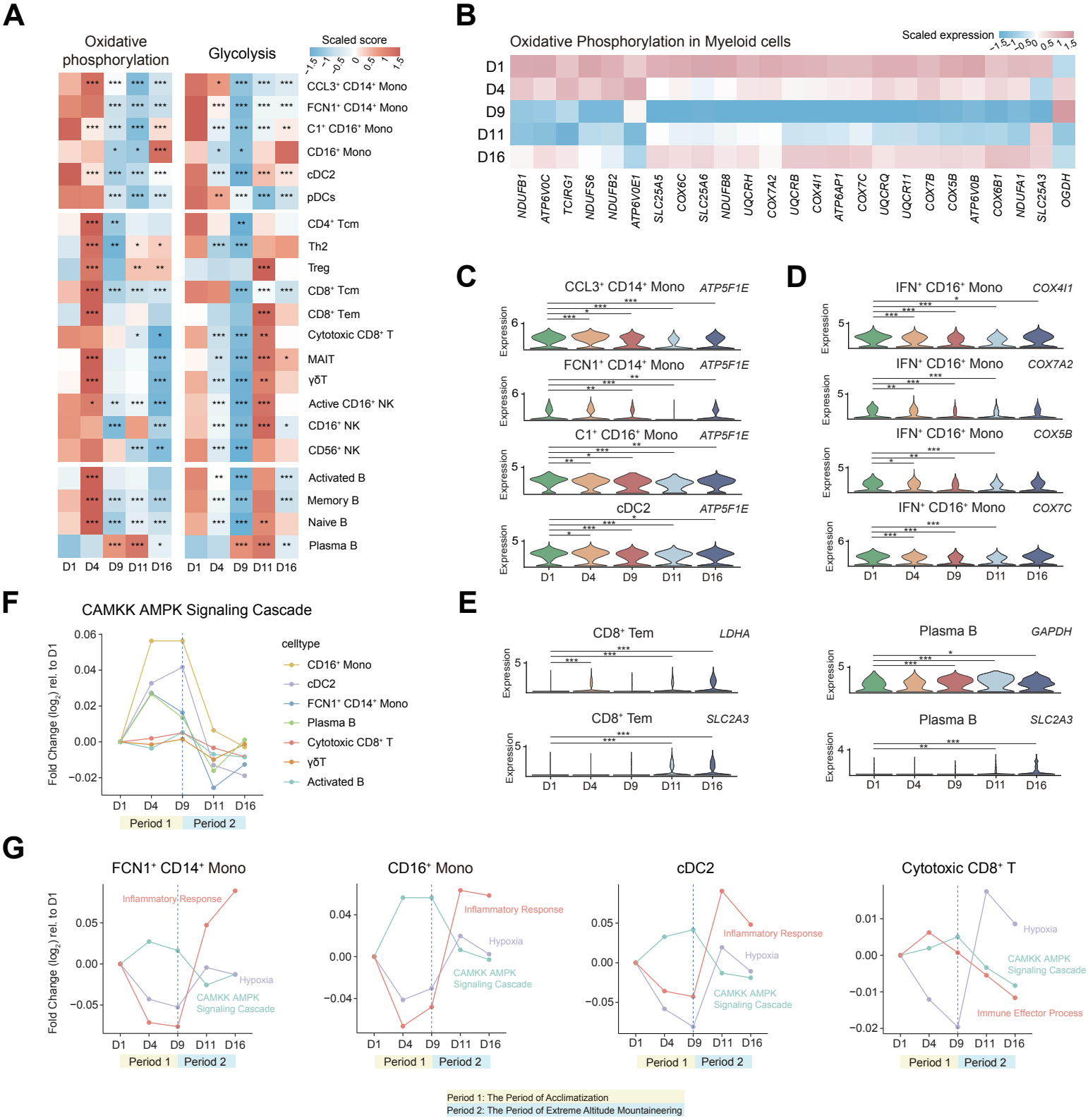
A
Oxidative phosphorylation
Glycolysis
Scaled score
CCL3⁺ CD14⁺ Mono
FCN1⁺ CD14⁺ Mono
C1⁺ CD16⁺ Mono
CD16⁺ Mono
cDC2
pDCs
CD4⁺ Tcm
Th2
Treg
CD8⁺ Tcm
CD8⁺ Tem
Cytotoxic CD8⁺ T
MAIT
γδT
Active CD16⁺ NK
CD16⁺ NK
CD56⁺ NK
Activated B
Memory B
Naive B
Plasma B
D1 D4 D9 D11 D16
B
Oxidative Phosphorylation in Myeloid cells
Scaled expression
D1
D4
D9
D11
D16
NDUFB1 ATP6V0C TCIRG1 NDUFS6 NDUFB2 ATP6V0E1 SLC25A5 COX6C SLC25A6 NDUFB8 UQCRH COX7A2 UQCRB COX4I1 ATP6AP1 COX7C UQCRQ UQCR11 COX7B COX5B ATP6V0B COX6B1 NDUFA1 SLC25A3 OGDH
C
CCL3⁺ CD14⁺ Mono ATP5F1E
FCN1⁺ CD14⁺ Mono ATP5F1E
C1⁺ CD16⁺ Mono ATP5F1E
cDC2 ATP5F1E
Expression
D
IFN⁺ CD16⁺ Mono COX4I1
IFN⁺ CD16⁺ Mono COX7A2
IFN⁺ CD16⁺ Mono COX5B
IFN⁺ CD16⁺ Mono COX7C
F
CAMKK AMPK Signaling Cascade
Fold Change (log2) rel. to D1
celltype
CD16⁺ Mono
cDC2
FCN1⁺ CD14⁺ Mono
Plasma B
Cytotoxic CD8⁺ T
γδT
Activated B
Period 1
Period 2
E
CD8⁺ Tem LDHA
CD8⁺ Tem SLC2A3
Plasma B GAPDH
Plasma B SLC2A3
G
FCN1⁺ CD14⁺ Mono
CD16⁺ Mono
cDC2
Cytotoxic CD8⁺ T
Inflammatory Response
Hypoxia
CAMKK AMPK Signaling Cascade
Immune Effector Process
Period 1: The Period of Acclimatization
Period 2: The Period of Extreme Altitude Mountaineering

Figure 6

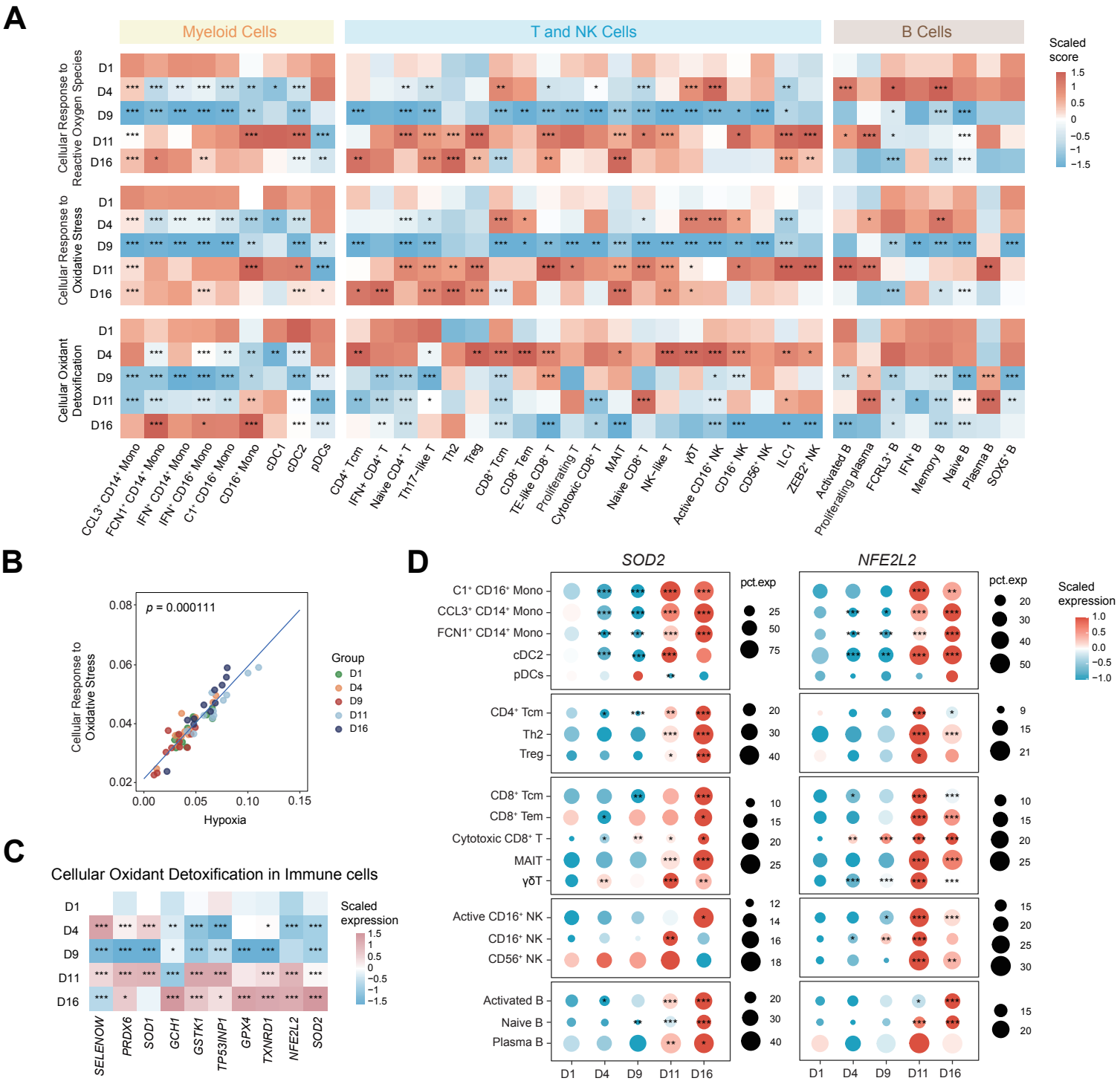
A
Myeloid Cells
T and NK Cells
B Cells
Scaled score
Cellular Response to Reactive Oxygen Species
Cellular Response to Oxidative Stress
Cellular Oxidant Detoxification
D1
D4
D9
D11
D16
CCL3+ CD14+ Mono
FCN1+ CD14+ Mono
IFN+ CD14+ Mono
IFN+ CD16+ Mono
C1+ CD16+ Mono
CD16+ Mono
cDC1
cDC2
pDCs
CD4+ Tcm
IFN+ CD4+ T
Naive CD4+ T
Th17-like T
Th2
Treg
CD8+ Tcm
CD8+ Tem
TE-like CD8+ T
Proliferating T
Cytotoxic CD8+ T
MAIT
Naive CD8+ T
NK-like T
γδT
Active CD16+ NK
CD16+ NK
CD56+ NK
ILC1
ZEB2+ NK
Activated B
Proliferating plasma
FCRL3+ B
IFN+ B
Memory B
Naive B
Plasma B
SOX5+ B
B
p = 0.000111
Cellular Response to Oxidative Stress
Hypoxia
Group
D1
D4
D9
D11
D16
C
Cellular Oxidant Detoxification in Immune cells
Scaled expression
SELENOW
PRDX6
SOD1
GCH1
GSTK1
TP53INP1
GPX4
TXNRD1
NFE2L2
SOD2
D
SOD2
NFE2L2
pct.exp
Scaled expression
C1+ CD16+ Mono
CCL3+ CD14+ Mono
FCN1+ CD14+ Mono
cDC2
pDCs
CD4+ Tcm
Th2
Treg
CD8+ Tcm
CD8+ Tem
Cytotoxic CD8+ T
MAIT
γδT
Active CD16+ NK
CD16+ NK
CD56+ NK
Activated B
Naive B
Plasma B
D1
D4
D9
D11
D16

Figure 7

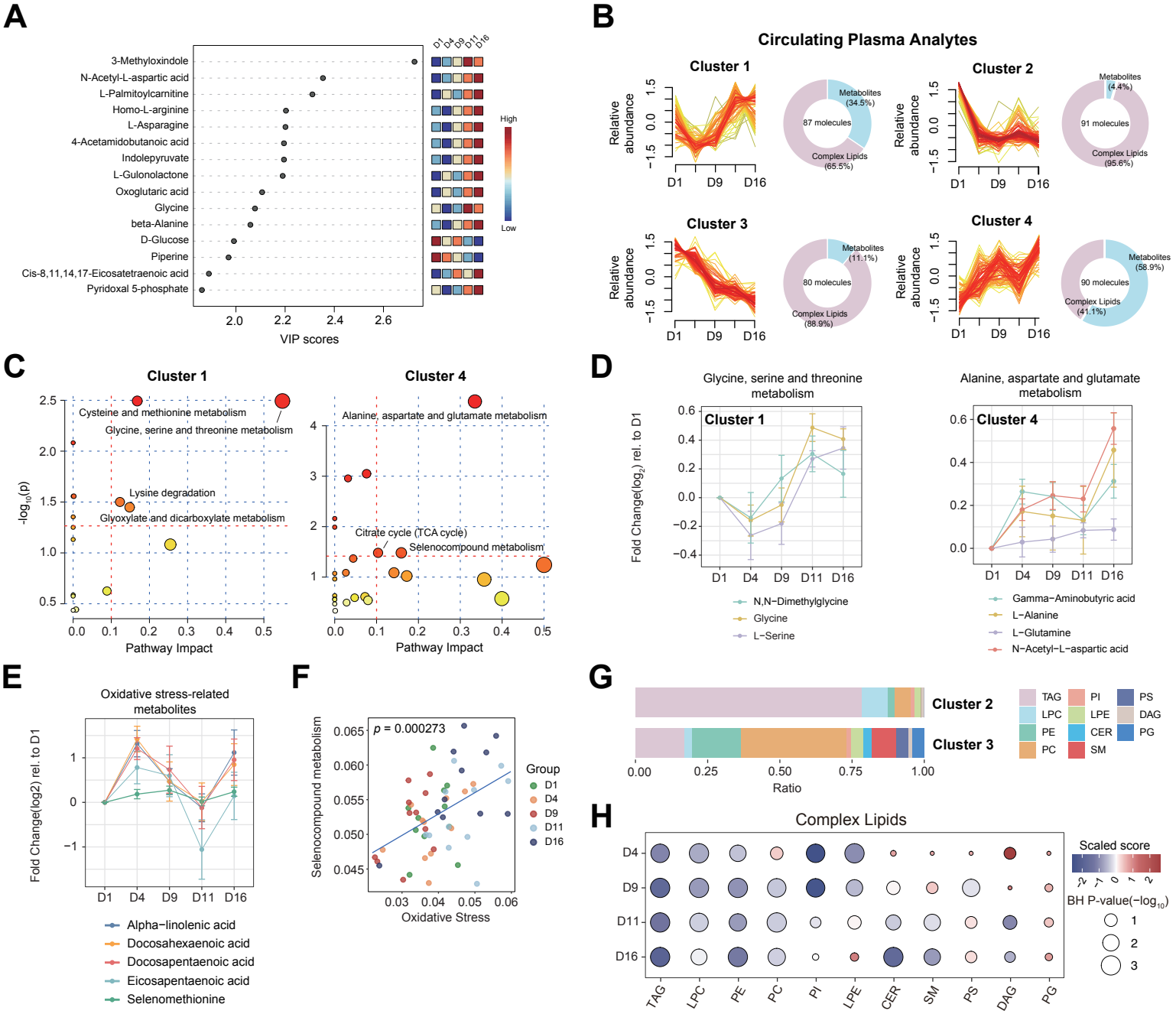
A
3-Methyloxindole
N-Acetyl-L-aspartic acid
L-Palmitoylcarnitine
Homo-L-arginine
L-Asparagine
4-Acetamidobutanoic acid
Indolepyruvate
L-Gulonolactone
Oxoglutaric acid
Glycine
beta-Alanine
D-Glucose
Piperine
Cis-8,11,14,17-Eicosatetraenoic acid
Pyridoxal 5-phosphate
D1 D4 D9 D11 D16
High
Low
VIP scores
B
Circulating Plasma Analytes
Cluster 1
Cluster 2
Cluster 3
Cluster 4
Relative abundance
Metabolites (34.5%)
87 molecules
Complex Lipids (65.5%)
Metabolites (4.4%)
91 molecules
Complex Lipids (95.6%)
Metabolites (11.1%)
80 molecules
Complex Lipids (88.9%)
Metabolites (58.9%)
90 molecules
Complex Lipids (41.1%)
C
Cluster 1
Cluster 4
Cysteine and methionine metabolism
Glycine, serine and threonine metabolism
Lysine degradation
Glyoxylate and dicarboxylate metabolism
Alanine, aspartate and glutamate metabolism
Citrate cycle (TCA cycle)
Selenocompound metabolism
Pathway Impact
D
Glycine, serine and threonine metabolism
Alanine, aspartate and glutamate metabolism
Fold Change(log2) rel. to D1
N,N−Dimethylglycine
Glycine
L−Serine
Gamma−Aminobutyric acid
L−Alanine
L−Glutamine
N−Acetyl−L−aspartic acid
E
Oxidative stress-related metabolites
Alpha−linolenic acid
Docosahexaenoic acid
Docosapentaenoic acid
Eicosapentaenoic acid
Selenomethionine
F
p = 0.000273
Selenocompound metabolism
Oxidative Stress
Group
D1
D4
D9
D11
D16
G
Cluster 2
Cluster 3
Ratio
TAG
LPC
PE
PC
PI
LPE
CER
SM
PS
DAG
PG
H
Complex Lipids
Scaled score
BH P-value(−log10)

Supplemental Figure 1

A

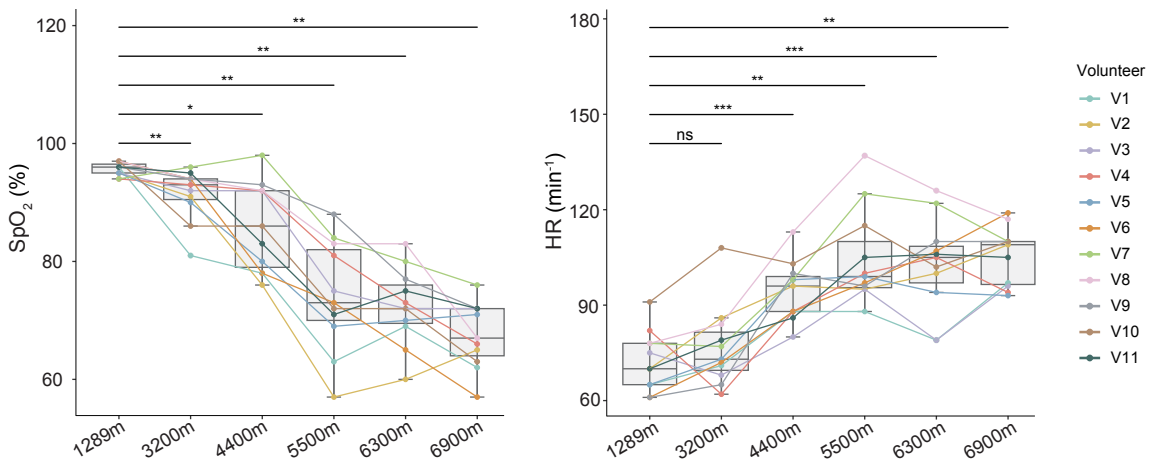

B

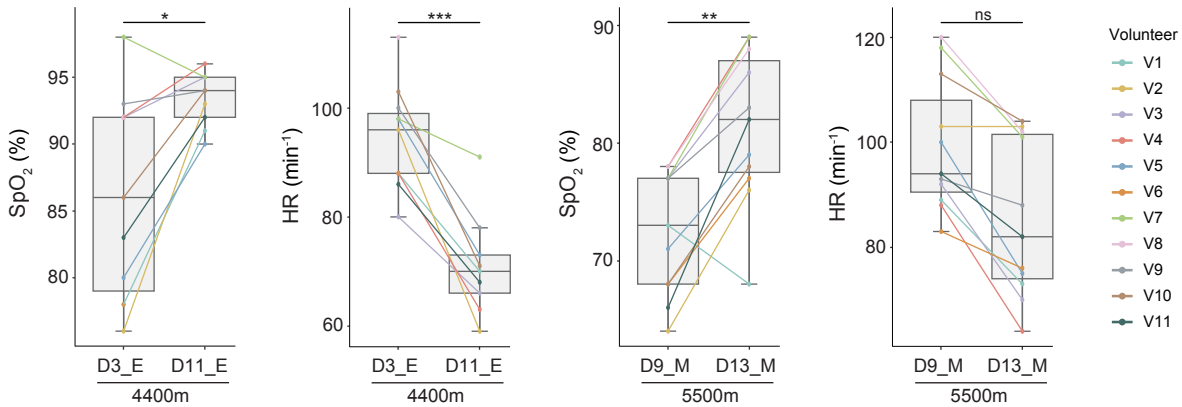

C

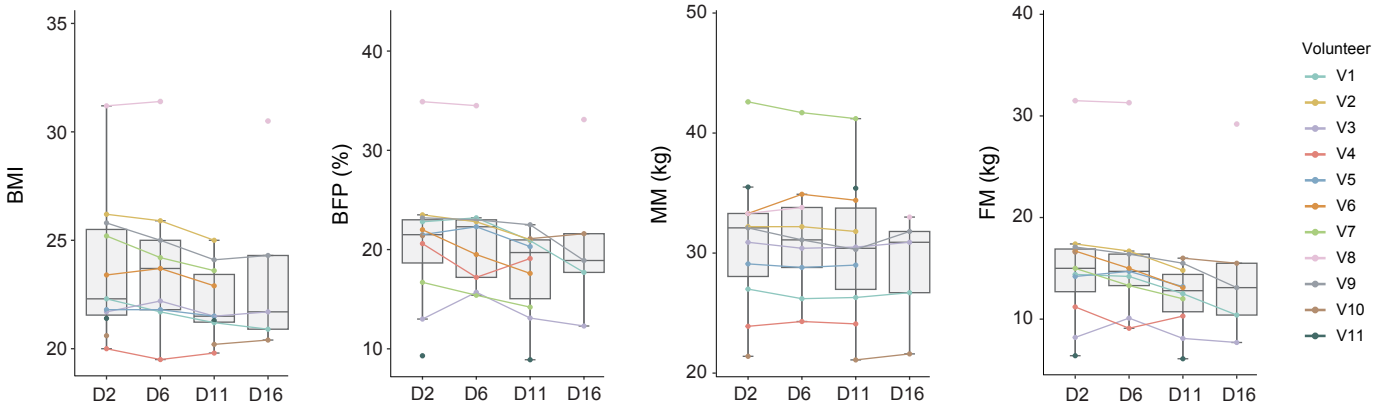

Supplemental Figure 2

Red Blood Cell Related Parameters

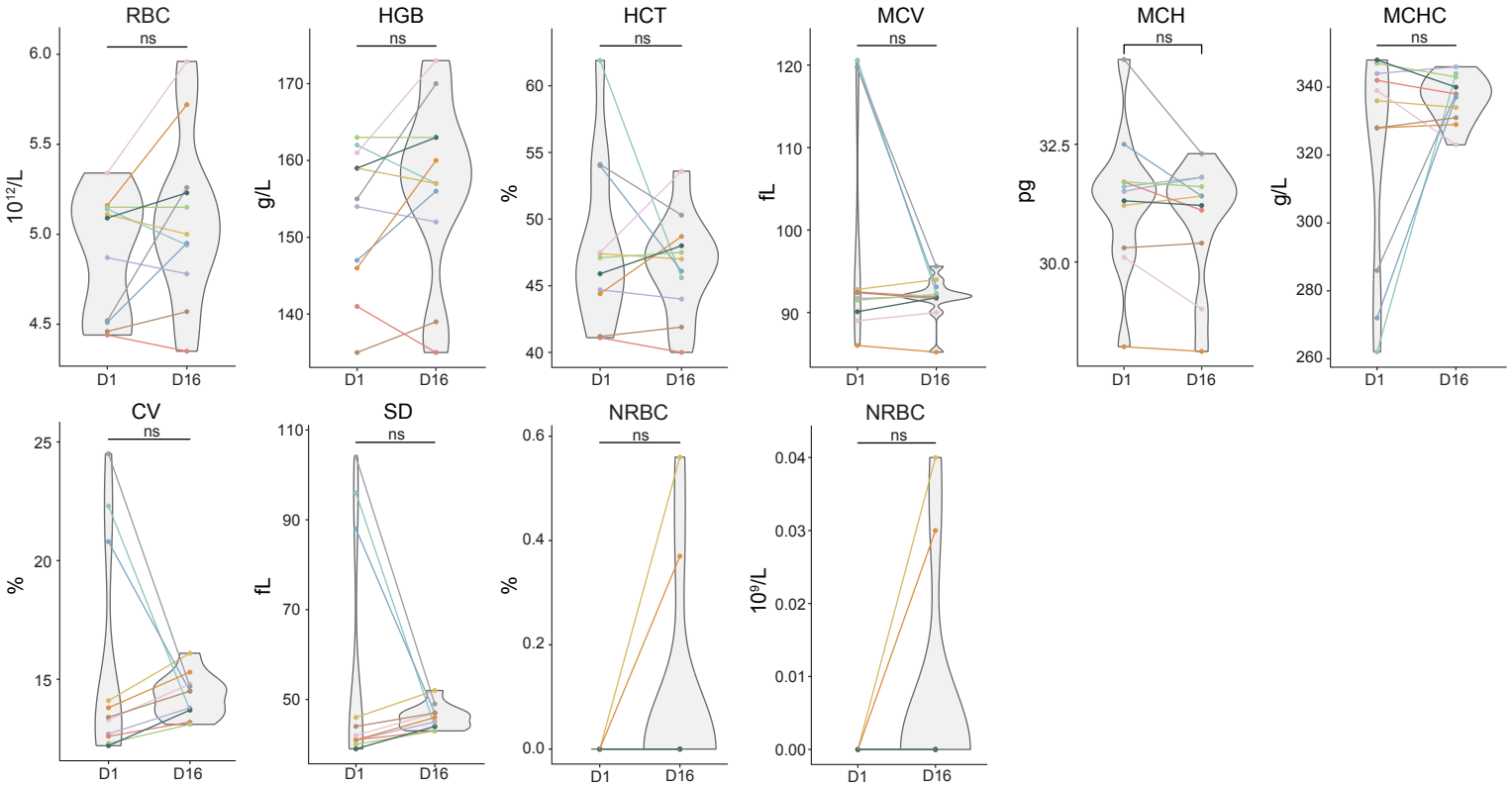

Platelet Related Parameters

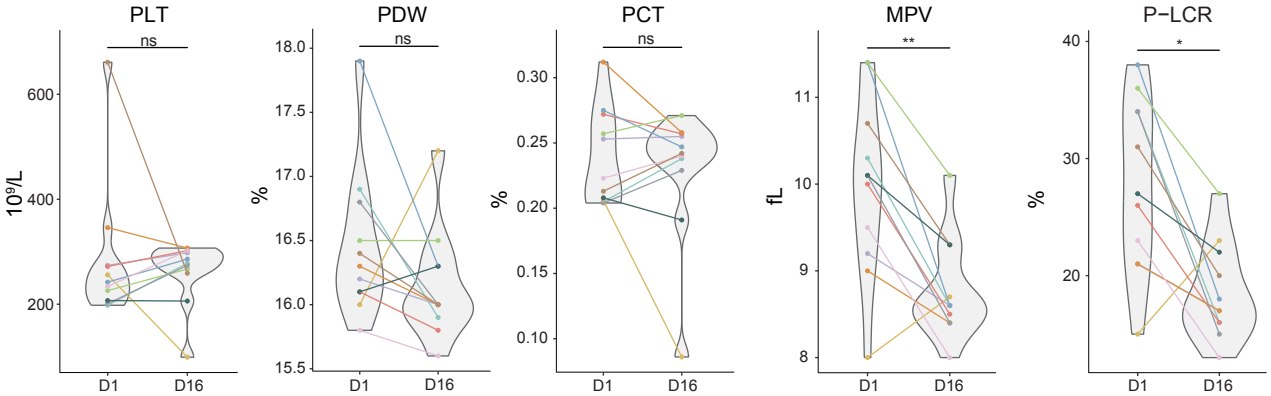

White Blood Cell Related Parameters

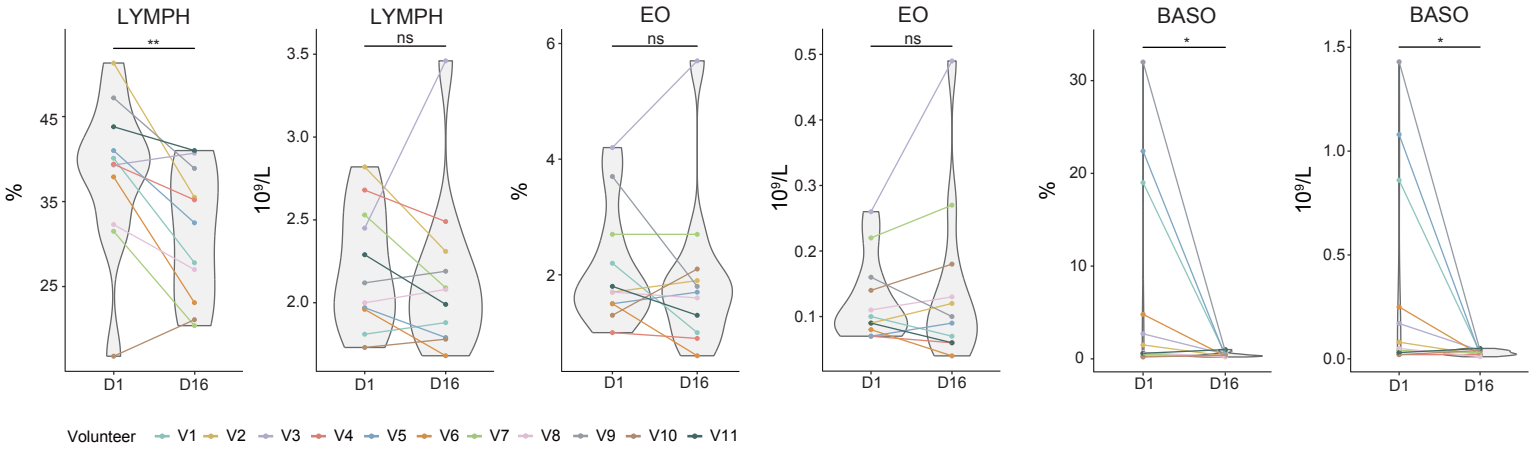

Supplemental Figure 3

A

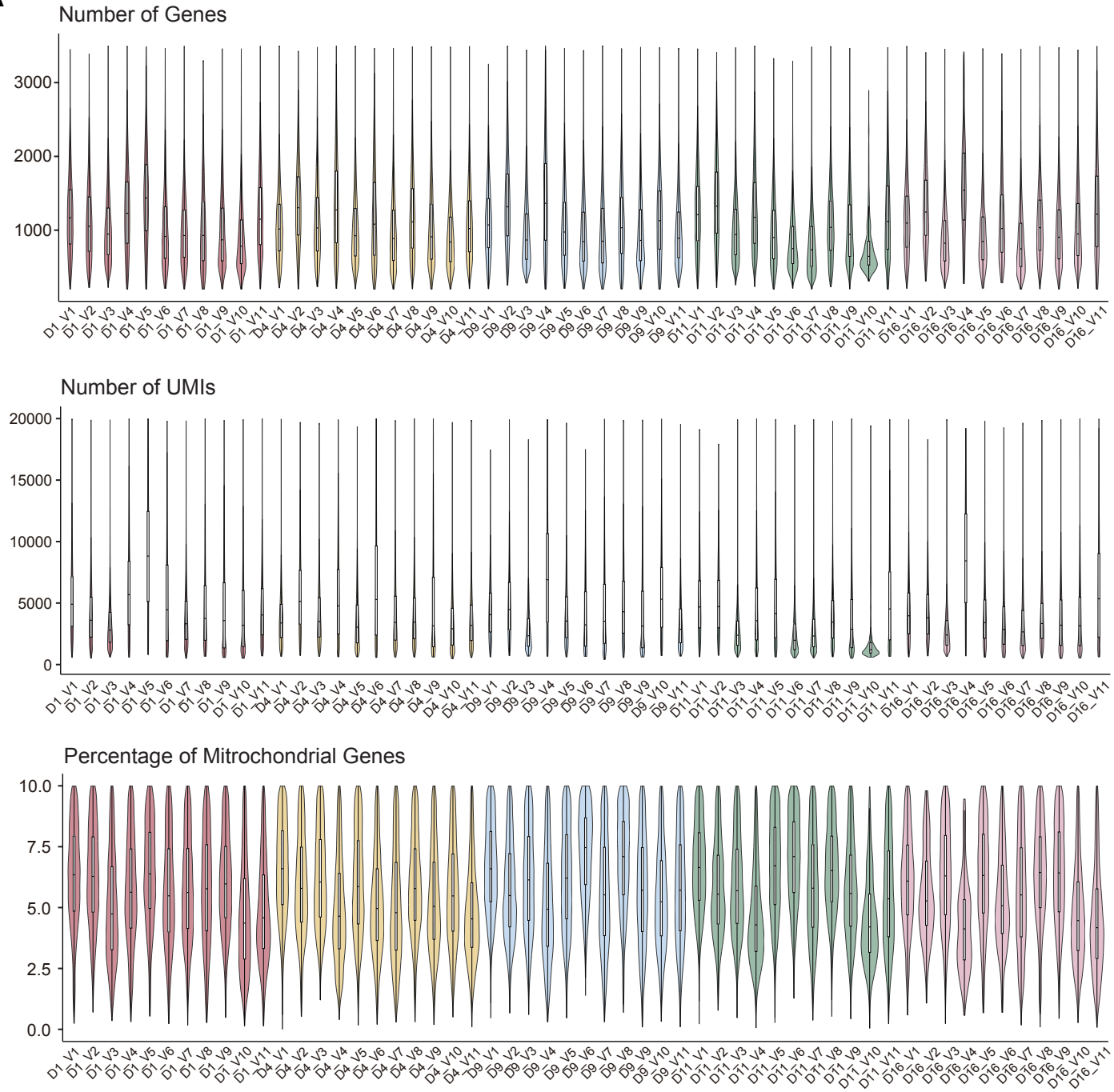

B

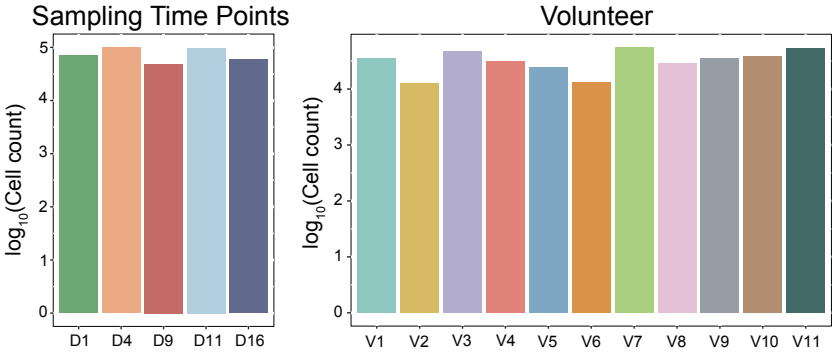

Supplemental Figure 4

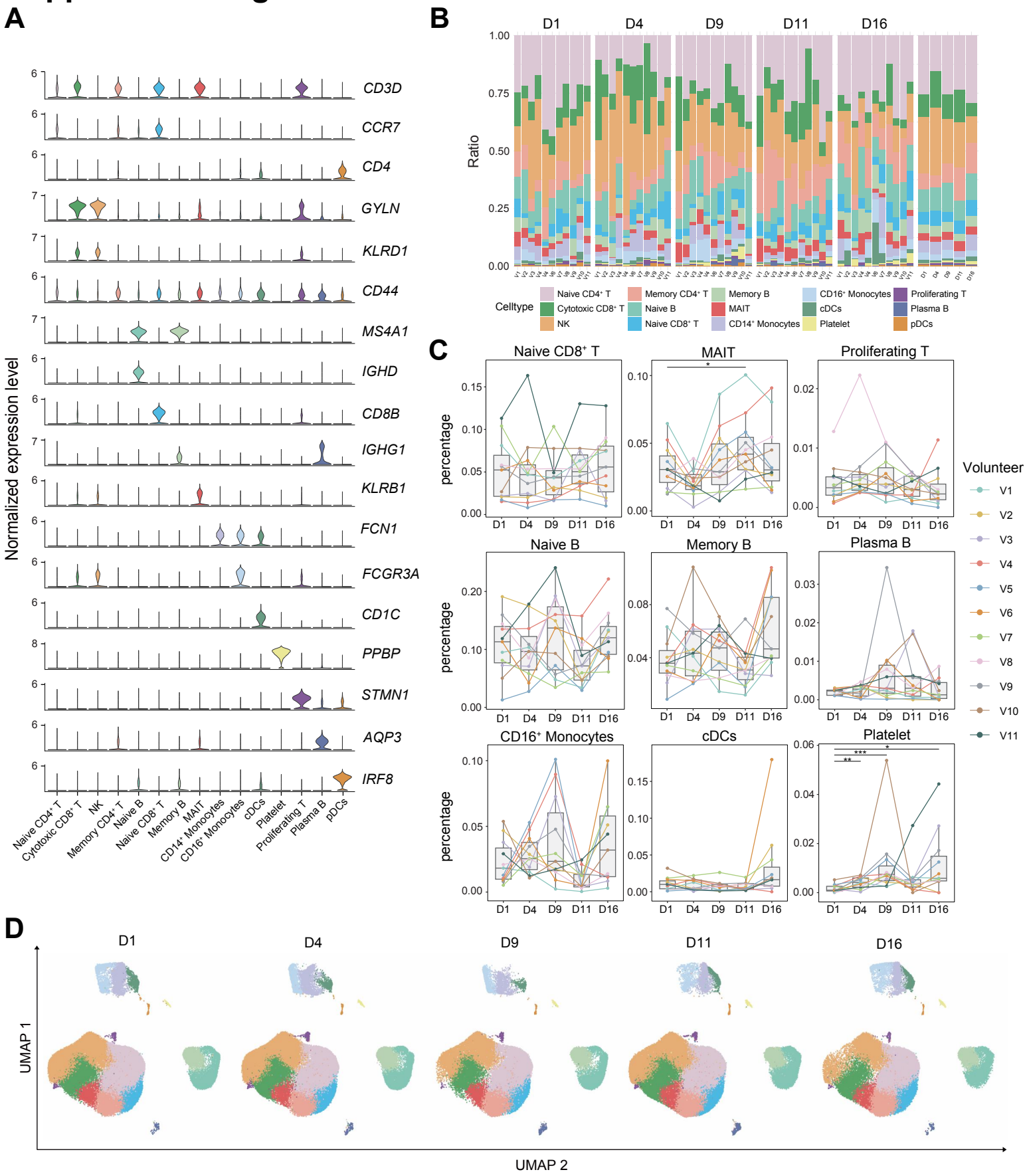

Supplemental Figure 5

Supplemental Figure 6

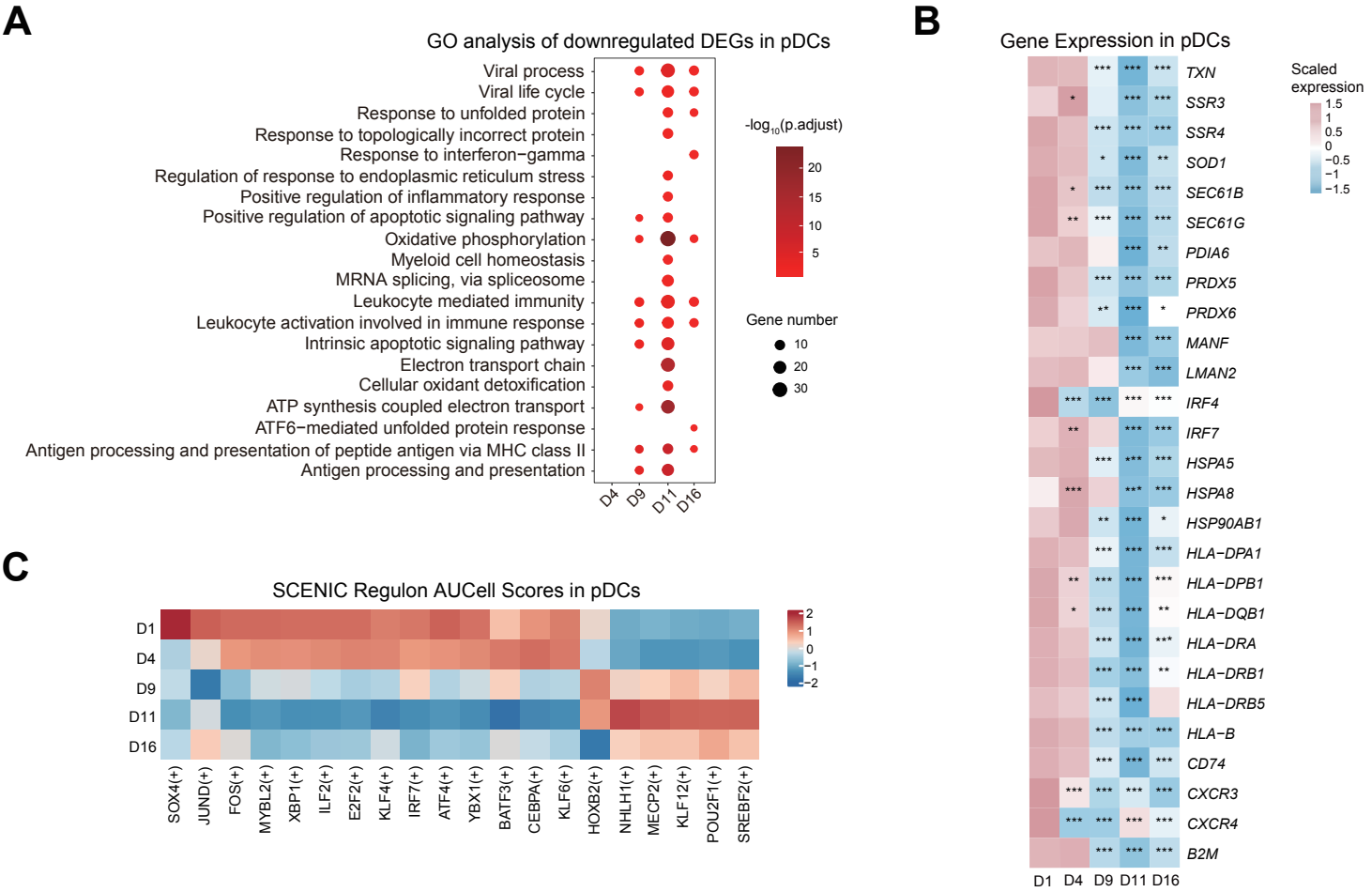

Supplemental Figure 7

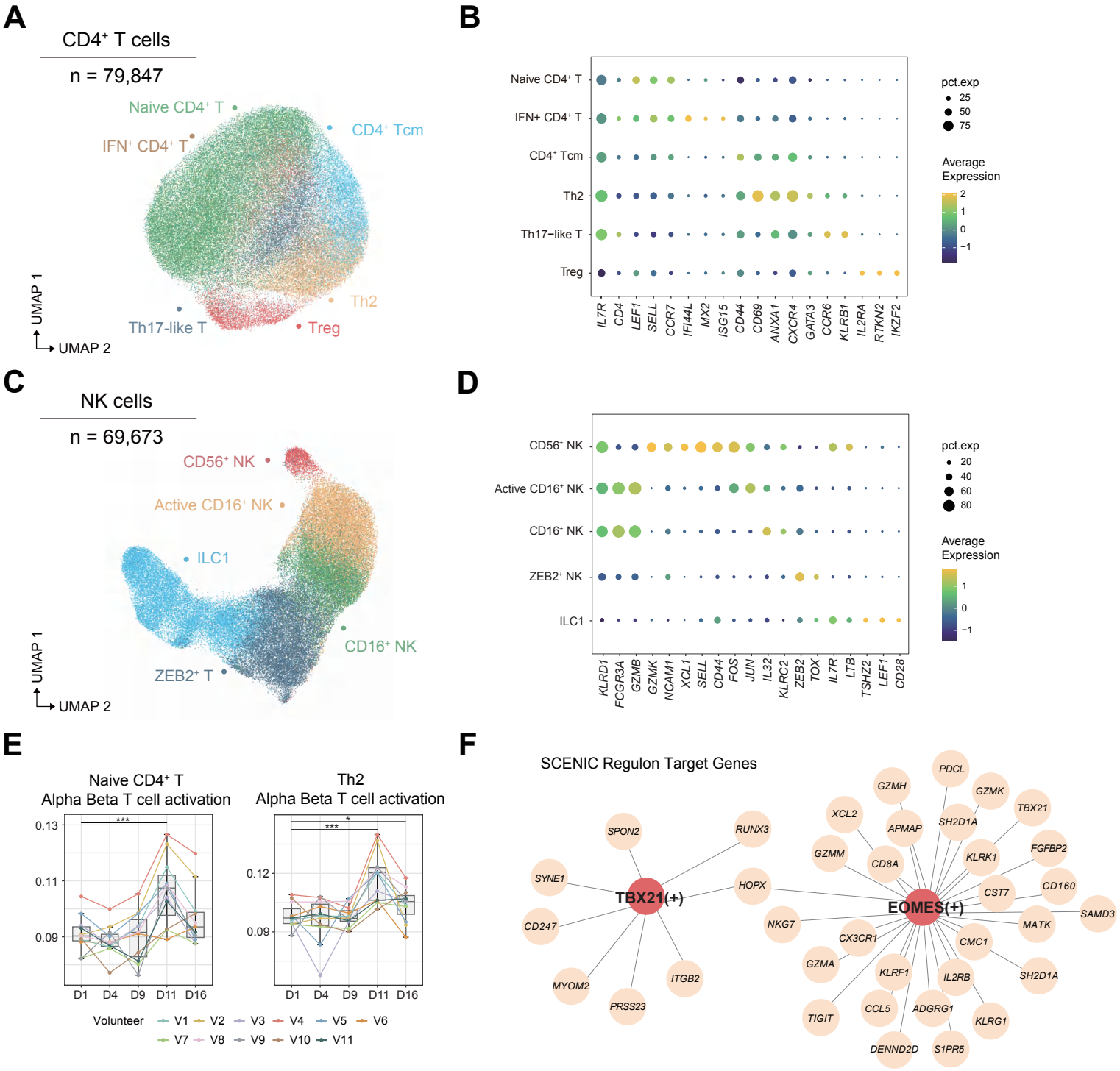

Supplemental Figure 8

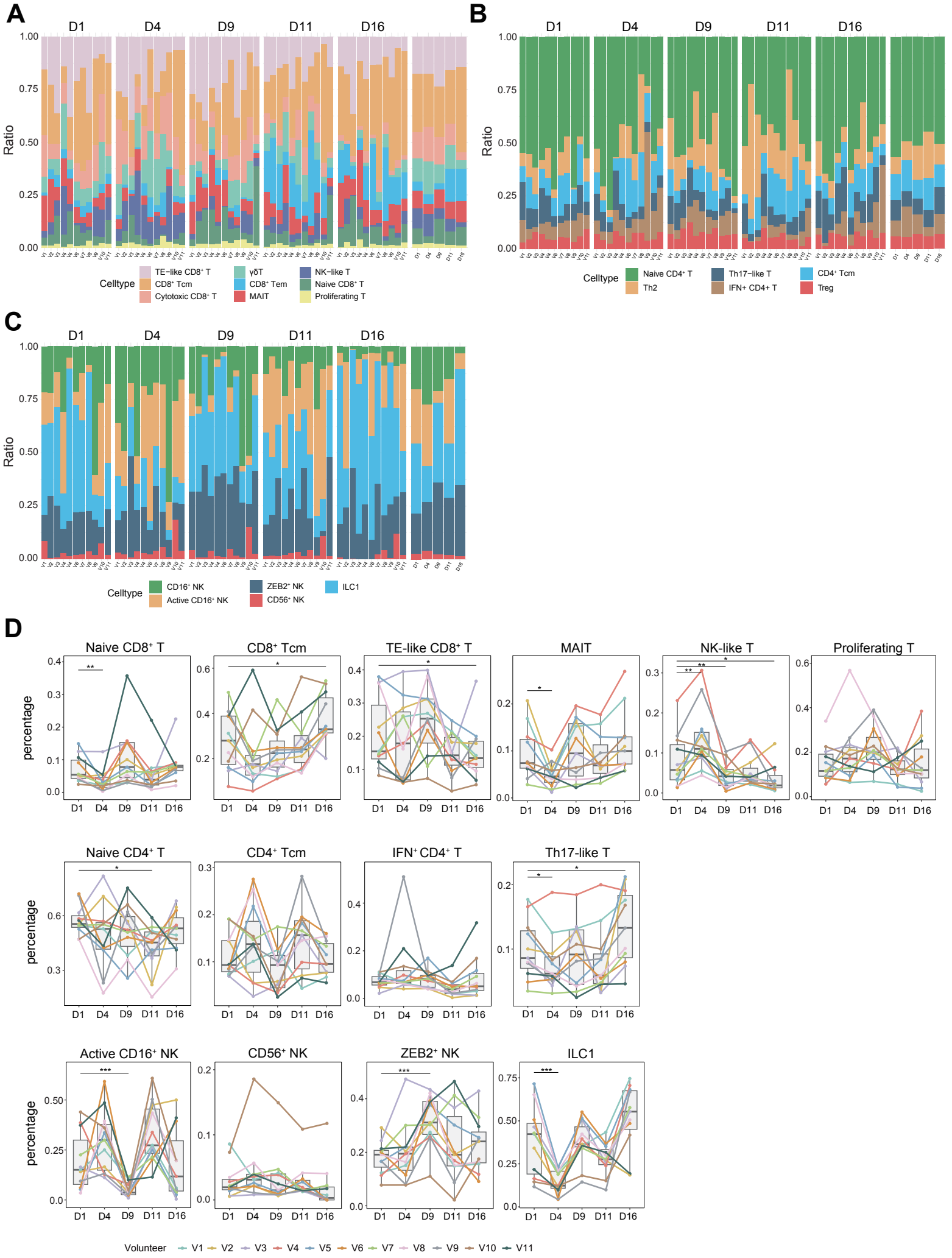

Supplemental Figure 9

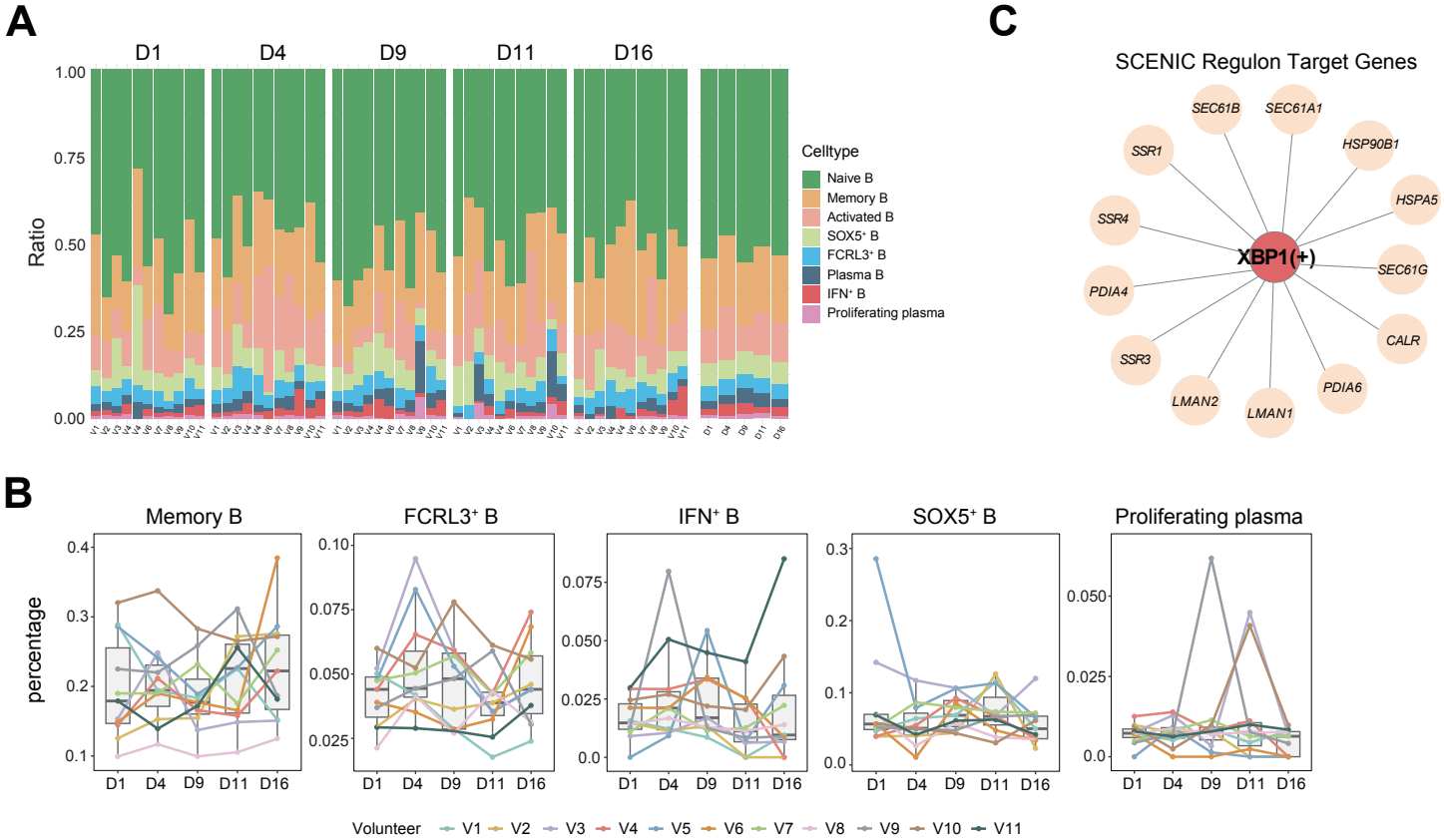

Supplemental Figure 10

A

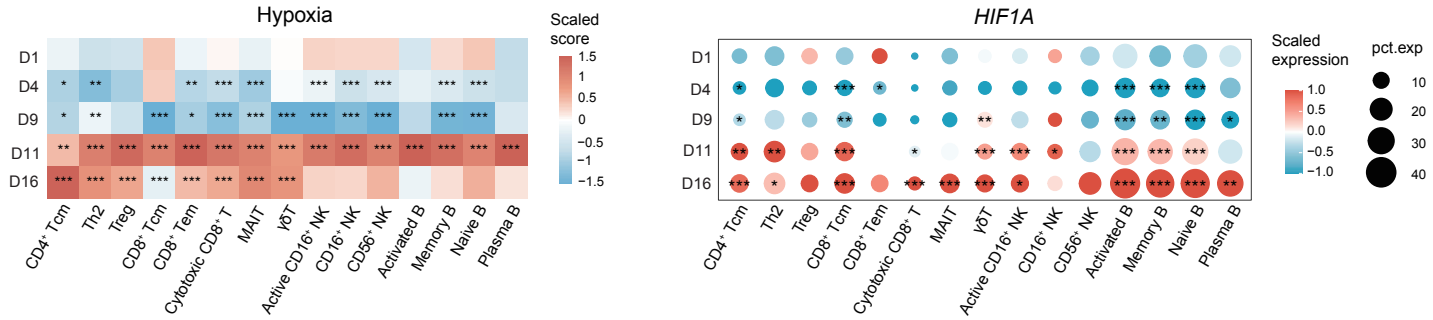

B

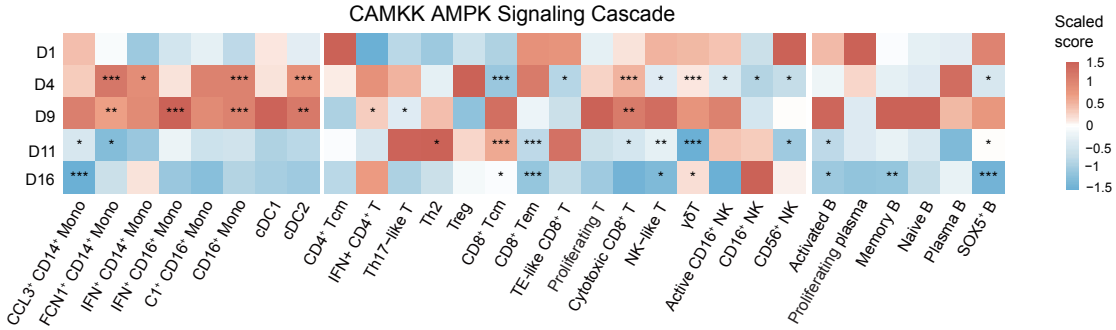

C

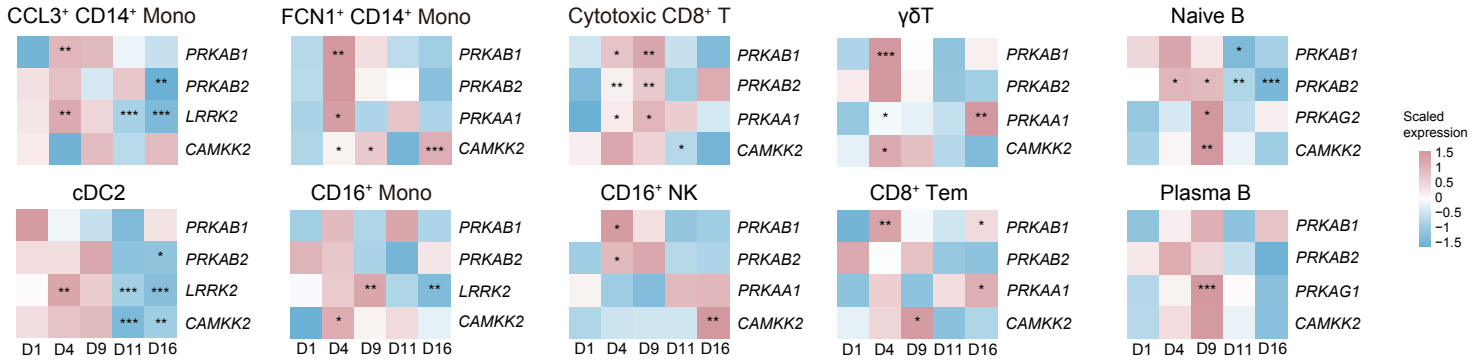

Supplemental Figure 11

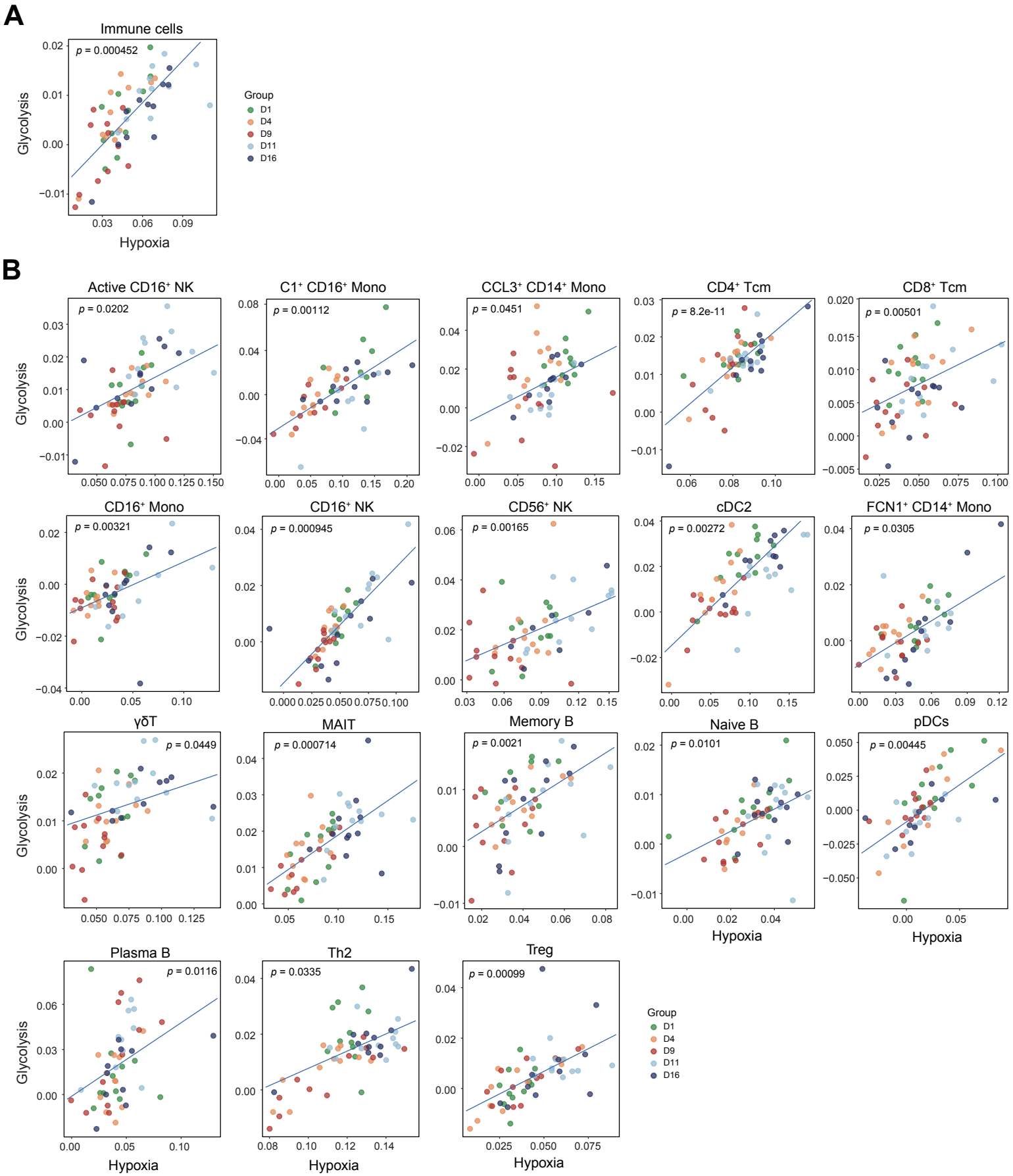
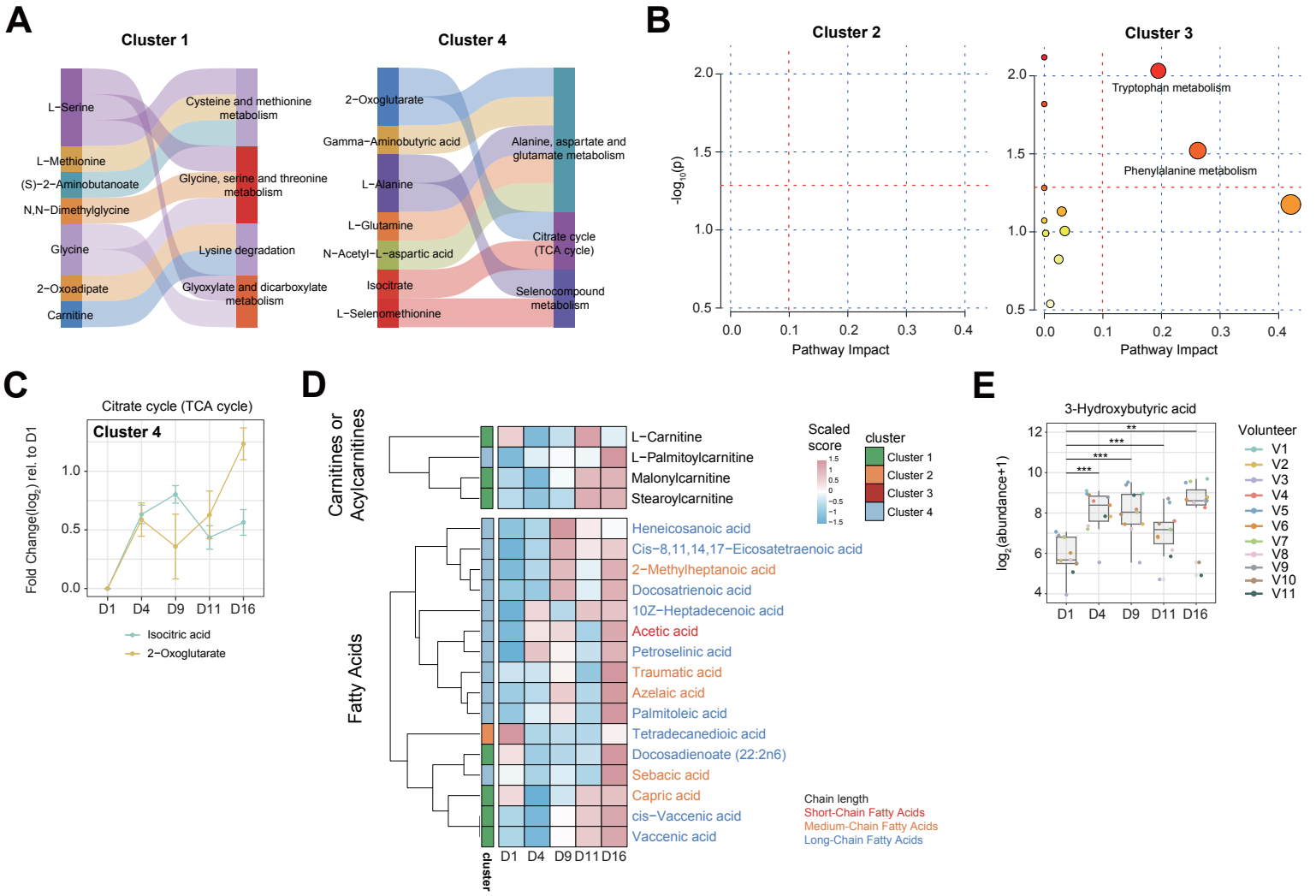
Supplemental Figure 12